12-1-2017

Evaluating Spatial Variability in Sediment and Phosphorus Concentration-Discharge Relationships Using Bayesian Inference and Self-Organizing Maps

Kristen L. Underwood
University of Vermont

Donna M. Rizzo
University of Vermont

Andrew W. Schroth
University of Vermont

Mandar M. Dewoolkar
University of Vermont

Recommended Citation

Evaluating Spatial Variability in Sediment and Phosphorus Concentration-Discharge Relationships Using Bayesian Inference and Self-Organizing Maps

Kristen L. Underwood[1] (iD), **Donna M. Rizzo[1], Andrew W. Schroth[2]** (iD)**, and Mandar M. Dewoolkar[1]**

[1]Civil & Environmental Engineering, University of Vermont, Burlington, VT, USA, [2]Department of Geology, University of Vermont, Burlington, VT, USA

Abstract Given the variable biogeochemical, physical, and hydrological processes driving fluvial sediment and nutrient export, the water science and management communities need data-driven methods to identify regions prone to production and transport under variable hydrometeorological conditions. We use Bayesian analysis to segment concentration-discharge linear regression models for total suspended solids (TSS) and particulate and dissolved phosphorus (PP, DP) using 22 years of monitoring data from 18 Lake Champlain watersheds. Bayesian inference was leveraged to estimate segmented regression model parameters and identify threshold position. The identified threshold positions demonstrated a considerable range below and above the median discharge—which has been used previously as the default breakpoint in segmented regression models to discern differences between pre and post-threshold export regimes. We then applied a Self-Organizing Map (SOM), which partitioned the watersheds into clusters of TSS, PP, and DP export regimes using watershed characteristics, as well as Bayesian regression intercepts and slopes. A SOM defined two clusters of high-flux basins, one where PP flux was predominantly episodic and hydrologically driven; and another in which the sediment and nutrient sourcing and mobilization were more bimodal, resulting from both hydrologic processes at post-threshold discharges and reactive processes (e.g., nutrient cycling or lateral/vertical exchanges of fine sediment) at prethreshold discharges. A separate DP SOM defined two high-flux clusters exhibiting a bimodal concentration-discharge response, but driven by differing land use. Our novel framework shows promise as a tool with broad management application that provides insights into landscape drivers of riverine solute and sediment export.

1. Introduction

The river network is an integrator of spatiotemporal variability in catchment properties. Stakeholders face significant challenges to model the export of sediment and nutrients based on concentration-discharge relationships measured at a catchment outlet, and to prioritize the allocation of limited resources to achieve reductions in sediment and pollutant loading. Given the regulatory context of Total Maximum Daily Loads (TMDLs) in the United States and the Water Framework Directive in the European Union, there has been a recent focus on quantifying loads of solutes and sediment. Yet as research becomes increasingly interdisciplinary in nature, a more holistic approach to investigating catchment dynamics has returned emphasis to concentration-discharge relationships and what they may reveal about biogeochemical filtering processes at multiple spatiotemporal scales (Basu et al., 2011; Gall et al., 2013). Better understanding of concentration-discharge dynamics will help identify critical catchment locations and time periods ("hot spots" and "hot moments") responsible for disproportionate fluxes of solutes and sediment, inform best management practices, and thereby optimize overall reductions in loading at broader temporal and spatial scales (Heathwaite et al., 2000; McClain et al., 2003).

Practitioners need models that predict spatiotemporal variability in concentration-discharge relationships and their linkage to catchment characteristics and processes—and at the same time deal with large amounts of data that vary in type and spatial-temporal resolution. Physically based, distributed models are able to forecast constituent concentration and flux, but accuracy and calibration are resource-intensive, making such models typically less transferable among watersheds or regions (Todini, 2007). On the other hand, data-driven models can be more readily implemented and have the appeal of representing system

complexity in simple ways (McDonnell et al., 2007), although they are more limited in their prediction capabilities. Ideally, stakeholders are guided by a combination of model types. With the advent of automated samplers and in situ sensors, an increasing number of studies have leveraged high-frequency monitoring data to develop conceptual models that further refine our understanding of temporal and spatial patterns in concentration-discharge dynamics (e.g., Bende-Michl et al., 2013; Lloyd et al., 2016).

Parametric statistical techniques have been applied to infer relationships between water quality and various biogeochemical characteristics of catchments using concentration (C) –discharge (Q) or load-discharge relationships. The parsimonious sediment (and nutrient) rating curve—i.e., $\log(C) = \log(\beta_0) + \beta_1 \log(Q)$—has been used to examine between-watershed differences in sediment and solute production (e.g., Vogel et al., 2005; Walling, 1977). Sediment and nutrient regression parameters have been interpreted to suggest drivers of underlying processes (Asselman, 2000; Basu et al., 2011; Godsey et al., 2009; Syvitski et al., 2000). While prediction does not necessarily suggest causation, the coefficient ($\log \beta_0$) and exponent (β_1) in this linear model can be interpreted to suggest something about the system properties (Asselman, 2000; Syvitski et al., 2000) and encapsulate the "biogeochemical filtering" of the watershed in question (Gall et al., 2013). The intercept of the linear regression model represents the background sediment (or solute) concentration delivered from the catchment source regions and explained by variables other than changing discharge proximal to the gaging location. In the context of sediment transport modeling, the regression intercept reflects the capacity of the watershed to produce and transport fine sediment (Asselman, 2000). It has been characterized as an "index of sediment supply" (Wang et al., 2008) or a "baseline supply parameter" (Krishnaswamy et al., 2000), and may be a function of particle size and weathering intensity in the source catchment, as moderated by vegetative controls or human disturbances.

On the other hand, the regression slope parameter reflects the rate at which the energy of flowing water is transferred to its physical surroundings to entrain and transport sediment (or sediment-bound constituents) and to accomplish geomorphic change (Krishnaswamy et al., 2000; Wang et al., 2008). The regression slope can be thought of as an index of the river's erosive power, with higher values (i.e., steeper slopes) indicating greater sediment transport capacity, and may also reflect the degree to which additional sources of sediment (or sediment-related constituents) become available to the river at higher flow stages (Asselman, 2000). Flatter regression slopes can be characteristic of rivers where sediment continues to be transported even under lower discharge conditions—as a function of either ample supply or easily entrained particle size in the source areas, or both (Asselman, 2000). Previous studies have used the slope value from a concentration-discharge regression to classify catchments on a continuum between accretionary (> 0) and dilutionary (< 0) (Basu et al., 2010; Gall et al., 2013). Godsey et al. (2009) proposed that chemostatic watershed responses (i.e., constant concentration with increasing discharge) could be defined by an absolute value less than 0.2 (i.e., near-zero regression slope). Subsequent work (Basu et al., 2010; Thompson et al., 2011), however, clarified that at low slope values, constituent concentrations can still exhibit considerable variance around a central tendency (i.e., chemodynamic response). Moreover, as the slope value approaches zero, concentration becomes decoupled from discharge as an explanatory variable; the coefficient of determination (r^2) value becomes nonsignificant, and the linear regression slope loses importance in the interpretation of the concentration-discharge relationship.

Instead, the coefficient of variation (CV) ratio (i.e., CV of concentration versus CV of discharge) has been promoted to characterize the concentration-discharge relationship on a continuum from episodic (chemodynamic) to chemostatic (Thompson et al., 2011). Thompson et al. (2011) classified North American catchments with varying hydrologic, geologic, topographic, and land use settings based on a bivariate plot of CV ratio and normalized constituent export for total phosphorus and total suspended solids (among other constituents). Those watersheds with higher normalized export exhibited chemostasis (low CV ratios), which can be attributed to legacy stores of nutrients with an anthropogenic source (Basu et al., 2011) or geogenic constituents (Godsey et al., 2009). Building on this approach, Musolff et al. (2015) used a bivariate plot of CV ratios and regression slope to cluster humid temperate catchments into five constituent export regimes. Categories ranged from strongly chemodynamic responses, termed "threshold-driven" (with strongly positive regression slopes) or "reactive" (with smaller absolute values of the regression slope, either positive or negative), to less chemodynamic responses with a concentration-discharge correlation that is either weak ("chemostatic") or strong, ranging from accretionary (termed "mobilization") to "dilution" driven.
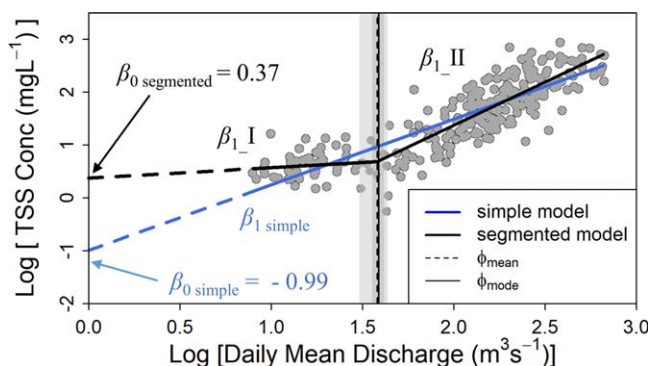
Figure 1. Comparison of best-fit simple (blue line) and segmented (black line) regression models for $\log_{10}$-transformed Total Suspended Solids (TSS) concentration versus daily mean discharge data for Winooski River (n = 261) for 1992–2015. Data points were fit with Bayesian linear regression methods. Threshold (φ) of segmented model depicted as solid vertical line (mode) and dashed vertical line (mean) with gray shading indicating the 95% credible interval of the posterior distribution. Regression parameters are annotated, including the intercept (β_0) for each model, and prethreshold ($\beta_{1\_}I$) and post-threshold slopes ($\beta_{1\_}II$) of the segmented model.

These studies employed slope and intercept parameters developed from simple linear regression models. Often, however, concentration-discharge (C-Q) relationships show variability across the discharge distribution (Zhang et al., 2016) or exhibit threshold effects (Meybeck & Moatar, 2012) that would be better modeled with a segmented regression. Segmented linear C-Q responses may result from temporal or spatial discontinuities in sediment and solute transport—either from natural conditions (e.g., bedrock nickpoints, or sudden reduction in gradient) or human modifications (e.g., dams) (Toone et al., 2014; Wang et al., 2008; Williams & Wolman, 1984). A segmented linear pattern may also result from sudden depletion of sediment/solute supply relative to discharge, or dilution effects (Meybeck & Moatar, 2012; Shanley et al., 2011).

Solute-export plots developed on slope and intercept parameters from simple regression models in the style of Musolff et al. (2015) or Thompson et al. (2011) may not adequately characterize solute export conditions for basins that exhibit significant threshold effects (Figure 1). Segments before and after a threshold will have different slope and intercept values, suggesting different sediment/solute export regimes (or functional stages) for pre and post-threshold flow conditions. Application of a segmented regression method will not only improve model fit, it can provide greater insight into landscape drivers of the C-Q response, and suggest management strategies appropriate to different functional stages (Bende-Michl et al., 2013).

However, it can be difficult to determine the optimal discharge value for the onset of threshold effects, and to identify the nature of the transition as either stepped, transitional, or continuous (Qian & Cuffney, 2012). Moatar et al. (2017) have presented a review of nine, single-threshold, C-Q patterns based on fixed segmentation at the median discharge value on a log-log plot (Meybeck & Moatar, 2012), although they acknowledge the actual inflection point in the slope of the C-Q relationship may vary from the median Q value. Methods have been developed to define a threshold using both parametric (Ryan et al., 2002—bootstrapping) and Bayesian techniques (Alameddine et al., 2011; Qian & Cuffney, 2012; Qian & Richardson, 1997); but relatively few studies have focused on determining the hydrologic, hydraulic, and biogeochemical processes that may account for these threshold effects, or dominate during pre and post-threshold phases (Moatar et al., 2017; Ryan et al., 2002; Wang et al., 2008).

We use a Bayesian regression method in this work to facilitate selection of the threshold position, and quantify the uncertainty on the estimated threshold, as well as other regression parameters. Generation of a posterior joint distribution for each model parameter, and the ability to define a credible interval for the estimate at a chosen probability level, permits explicit estimation of uncertainties associated with the model selection and the data (e.g., variance introduced by sampling and analytical methods, Qian et al., 2005). This approach provides more information than a Frequentist approach to simple (or segmented) regression that generates a single point estimate of the central tendency of model parameters. Bayesian frameworks have the added advantage of allowing for nonnormal distribution of residuals and greater robustness to outliers (Gelman et al., 2004). Bayesian methods have been applied to estimate values of regression parameters for simple linear models of stage-discharge relationships (Moyeed & Clark, 2005); an eight-parameter load rating curve for nutrients (Vigiak & Bende-Michl, 2013), and segmented regression models for nitrogen-discharge patterns (Alameddine et al., 2011; Qian & Richardson, 1997).

C-Q dynamics result from a complex interaction of hydrologic, hydraulic, and biogeochemical processes. "Functional stages" of sediment and nutrient export have been defined using hierarchical clustering to result from unique combinations of source strength and connectivity, entrainment or mobilization conditions, and transport mechanisms; and these functional stages vary in both space and time (Bende-Michl et al., 2013). Self-organizing maps (SOMs) are data-driven, nonparametric techniques well-suited for classifying or clustering data of varying types (e.g., continuous, ordinal, nominal), scales, and distributions (Kohonen, 1990, 2001, 2013). SOMs have advantages over other methods for data visualization and interpretation (Alvarez-Guerra et al., 2008), and have demonstrated superior performance over parametric methods where

data contain outliers or exhibit high variance (Mangiameli et al., 1996). SOMs have been used to classify or cluster multivariate environmental data, including in-stream species richness (Park et al., 2003), fish community distribution patterns (Stojkovica et al., 2013), alluvial fan types (Karymbalis et al., 2010), lake chemistry data associated with harmful algal blooms (Pearce et al., 2011, 2013), estuary sediment samples (Alvarez-Guerra et al., 2008), watershed-based ecoregions (Tran et al., 2003), and riverine habitats (Fytilis & Rizzo, 2013). While SOMs have been applied to hydrologic time series data to classify runoff response (Ley et al., 2011), the authors are not aware of research that has applied a neural network to cluster basins into sediment and nutrient export regimes.

In this work, we combine the application of a Bayesian segmented linear regression technique paired with an SOM to cluster patterns in C-Q relationships as a function of catchment properties for a humid-temperate study area located in a previously glaciated, mountainous region of the Northeastern U.S. The purpose of this research was twofold: (1) to model threshold effects in C-Q regressions using Bayesian techniques to enhance the utility of regression metrics to suggest watershed variability in hydrologically and biogeochemically driven impacts on C-Q dynamics; and (2) examine the ability of various watershed metrics to predict C-Q relationships and characterize between-watershed comparisons of sediment and nutrient flux or concentration.

2. Methods

2.1. Study Area

The study area consists of 18 tributary basins of Lake Champlain that drain portions of Vermont and New York in the northeastern U.S., as well as the province of Quebec in Canada (Figure 2). In recent decades, this largely mesotrophic lake has been impacted by an increasing frequency of harmful algal blooms in its eutrophic bays, and is the subject of a TMDL for phosphorus (Smeltzer et al., 2012). Eighteen of the Lake Champlain tributaries have been monitored for more than 25 years (Medalie et al., 2012) and were selected for this study for their sufficient duration of flow gaging and water quality records (Kennard et al., 2010). The selected basins range in size from 137 to 2,754 km^2 and represent a wide range of geologic settings and land cover/land use conditions.

The Lake Champlain Basin (LCB) was previously glaciated, and spans biogeophysical regions from the Green Mountains in Vermont to the Adirondack Highlands in New York, separated by the Champlain Valley Lowland in the north-central basin and Taconic Mountains and Vermont Valley in the south end of the basin merging with the Hudson Valley Lowland (Stewart & MacClintock, 1969). Elevations in the study basins range from 1,339 m at Mount Mansfield in the Winooski Basin of Vermont, and 1,629 m at Mount Marcy in the Ausable River basin of New York, to 29 m at the average water level of Lake Champlain. The climate is characterized as humid temperate, with mean annual precipitation (MAP) ranging from over 1,270 mm along the north-south trending spine of the Green Mountains to a low of 813 mm in the Champlain Valley (Randall, 1996). Within a typical year, a majority of the runoff from Lake Champlain tributaries occurs between ice-out and late spring (Shanley & Denner, 1999). The hydrologic regime is characterized by variable hydrologic source areas attributed to saturation-excess flow regimes (Dunne & Black, 1970). Flow in some of the basins is regulated to varying degrees by hydroelectric dams that operate in run-of-river mode (supporting information Table S1). In recent years, these basins have been impacted by extreme events, including Tropical Storm Irene (August 2011) in central and southern Vermont and floods of 1996 and 1998 in northeastern New York.

2.2. Watershed Characteristics

Various hydrologic, topographic, geologic, and land use characteristics were developed for the 18 tributary basins (Table 1). Land use in the selected watersheds ranges from 3.3 to 54% agricultural and 33 to 89% forested. Urban land uses, including transportation corridors, range from 4.4 to 14% (Troy et al., 2007). Flow-normalized total suspended solids (TSS), particulate phosphorus (PP), and dissolved phosphorus (DP) flux and concentration data for each basin were compiled from Medalie (2014) for each available year (1990–2012 for PP and DP; 1992–2012 for TSS). PP was derived as the difference of measured total and DP (filtered to < 0.45 μm). Flow-normalization was achieved using *Weighted Regressions on Time, Discharge, and Season* (Hirsch et al., 2010); and data thus reflect interannual variability in constituent flux and concentration attributed to factors other than flow variability. To facilitate between-watershed comparisons, mean annual
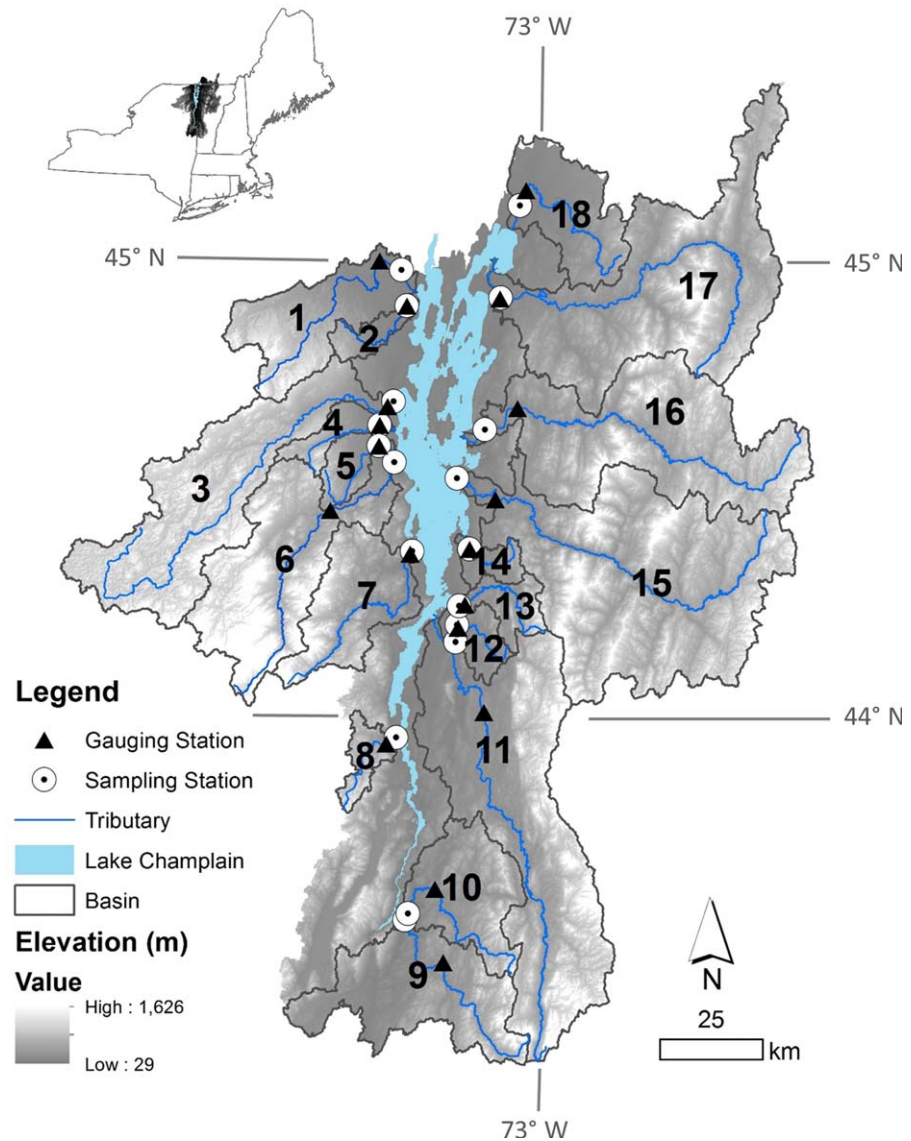
Figure 2. Locations of the 18 study area watersheds in the Lake Champlain Basin. Watershed identifications are keyed to Table 1.

constituent flux was normalized by basin area to generate a mean annual, flow-normalized, yield (in mT/km^2/yr for TSS and in kg/km^2/yr for PP and DP; supporting information Table S2).

Additionally, slope (β_1) and intercept ($\log_{10}[\beta_0]$) values from Bayesian linear regression models were developed for the time series of TSS, PP, and DP concentration (C) – discharge (Q) data (see next section). These data were included as indicators of the sediment and nutrient export regimes of the watersheds (Asselman, 2000; Vogel et al., 2005). C-Q data were sourced from long-term monitoring data sets of instantaneous concentrations (VTDEC, 2015) and daily mean flows (USGS, 2016). Velocity and depth-integrated composite samples were collected approximately monthly, targeting a mixture of flow conditions (VTDEC, 2015). PP/DP and TSS were sampled approximately 12 and 10 times per year, respectively. In the few cases (1.8% for TSS, 0.3% for DP/PP) where constituents were reported below the detection limit (i.e., 1 mg/L for TSS, 5 μg/L for DP/PP), a value one half the respective detection limit was substituted. C and Q data were $\log_{10}$–transformed to meet homoscedasticity assumptions for application of linear models.

Coefficient of Variation (CV) of the C and Q time series (nontransformed), were each calculated as the series standard deviation, σ, normalized by the series mean, μ:

Table 1
Physical Characteristics of Study Area Watersheds, Lake Champlain Basin

Map key	Tributary	Total drainage area[a] (km²)	Mean annual precipitation[b] (mm)	Peak flow anomaly[c]	Basin relief[d] (m)	Drainage density[e] (km/km²)	Percent of hydrologic soil group A & B soils[f] (%)	Land use[g]			
								Water/ wetland (%)	Forest (%)	Agriculture (%)	Developed (%)
6	Ausable	1,334	1,164	16.0	1,598	1.08	26.5	3.0	89.1	3.3	4.5
7	Bouquet	708	1,051	14.7	1,446	1.18	30.0	1.5	87.4	6.3	4.6
1	Great Chazy	778	848	11.8	1,139	1.54	38.7	3.7	68.7	21.9	5.6
16	Lamoille	1,870	1,198	10.7	1,309	1.89	24.4	2.3	39.1	44.4	14.2
14	LaPlatte	137	1,002	21.9	468	2.05	8.1	2.2	75.5	13.9	8.2
13	Lewis	207	1,074	19.1	736	2.32	28.5	4.2	61.6	25.6	8.2
5	Little Ausable	193	850	21.2	619	1.23	55.0	1.4	71.5	19.4	7.8
2	Little Chazy	140	917	14.1	429	1.37	45.1	3.5	58.4	30.7	7.3
12	Little Otter	188	974	14.7	380	3.08	15.2	3.4	33.0	54.0	9.4
9	Mettawee	1,063	1,228	17.7	1,117	1.36	25.6	2.7	59.1	29.3	8.9
17	Missisquoi	2,232	1,050	11.3	1,146	1.57	33.3	1.9	73.0	18.8	6.2
11	Otter	2,442	1,239	3.5	1,260	1.99	27.8	3.3	62.9	25.7	8.0
18	Pike	662	1,184	12.0	681	1.23	71.4	2.3	52.6	37.7	7.0
10	Poultney	719	1,120	15.3	800	1.65	13.0	5.0	66.0	20.9	8.0
8	Putnam	160	1,103	17.6	678	1.33	36.2	4.2	87.2	3.8	4.4
4	Salmon	175	913	20.1	693	1.42	55.4	2.2	77.9	11.0	9.0
3	Saranac	1,589	1,070	6.1	1,451	0.93	26.6	9.8	81.0	3.9	5.3
15	Winooski	2,754	1,163	10.3	1,307	1.77	18.1	1.5	76.6	9.9	11.7

[a]Source: (WBD) 1:24,000 scale.
[b]PRISM data for 1981–2010 obtained through USGS Streamstats of Vermont (Olson, 2014) and New York (Lumia et al., 2006).
[c]Ratio of mean annual peak flow to mean annual flow for the period from 1990 to 2012 (except Little Ausable (wy1992–2012) and Pike (wy2001–2015)).
[d]Source: 10 m Digital Elevation Models.
[e]Total length of National Hydrography Data set (NY, Que) or Vermont Hydrography Data set stream network mapped in each basin, normalized by basin area.
[f]Sources: SSURGO (NY and VT), Canadian National Soil Database (Que), and STATSGO02 (Franklin County portion of the Saranac River basin in NY).
[g]Source date: 2001; Developed category includes Open-Urban and Roads; Agriculture includes Brush/Transitional; from Troy et al. (2007).

$$CV = \frac{\sigma}{\mu}.$$

A CV ratio was then generated to evaluate the temporal inequality between CV of the two variables, C and Q:

$$\frac{CV_C}{CV_Q} = \frac{\sigma_C}{\mu_C} * \frac{\mu_Q}{\sigma_Q}.$$

Pre and post-threshold values (i.e., Segment I and II of the segmented regression model; Figure 1) were treated independently.

A flow duration curve for each basin was constructed from existing USGS records of mean daily Q for years 1990 through 2015 (Centre d'Expertise Hydrique Québec, 2016; Medalie, 2014; USGS, 2016). The threshold value determined from Bayesian linear regression (next section) was normalized in two ways to enable between-basin comparisons of the threshold magnitude: (a) as a ration to the median Q; and (b) expressed as a quantile of flow based on the flow duration curve.

2.3. Bayesian Linear Regression
2.3.1. Model Development

Segmented rating curves were developed via Bayesian linear regression (BLR) methods on the time series of C data (TSS, PP, DP) and mean daily Q data from the 18 tributaries for years 1990 through 2015. BLR provided a framework for identifying thresholds (Qian & Cuffney, 2012), and defining credible intervals around the estimated values for threshold, intercept, and pre and post-threshold slopes (Figure 1). Bayesian models also permitted the seamless back-transformation of error terms addressing bias introduced when using log-transformed regressors (Koch & Smillie, 1986; Stow et al., 2006), and allowed for the explicit estimation of sources of uncertainty in the C-Q relationships (Schmelter et al., 2012). Concentration was modeled as a power function of discharge:

$$C_t = \beta_0 \ Q_t^{\beta_1},$$

where C is the sediment or solute concentration, and Q is the river discharge for a specified time interval, t. Rating curves were developed as the logarithm (base 10) of instantaneous concentration, C, regressed on the $\log_{10}$ of daily mean discharge, Q:

$$log_{10}C_t = log_{10}\beta_0 + \beta_1 log_{10}(Q_t) + \varepsilon.$$

Log_{10} (β_0)—commonly simplified to β_0—is the model intercept and β_1 is the slope of the regression line, which describes the predicted change in log-C with each incremental increase in log-Q. The error term, ε, then reflects scatter about the regression line and encapsulates all other sources of variance in sediment (nutrient) C with Q, such as differences in constituent availability due to seasonal effects and antecedent conditions. This error term also includes measurement error of model parameters. The following segmented linear regression model was applied to all time series data:

$$y \sim N(\mu_y, \sigma_y^2), \text{where} :$$

$$\mu_y = \begin{cases} \beta_0 + \beta_1 \ x + \varepsilon_1 & \text{if } x < \phi \ (Segment \ I) \\ \beta_0 + (\beta_1 + \delta) \ x + \varepsilon_2 & \text{if } x \geq \phi \ (Segment \ II) \end{cases}$$

and where y refers to the response variable ($\log_{10}$ C); x is the explanatory variable ($\log_{10}$ Q); μ_y and σ_y^2 are the mean and variance of the response variable, respectively; ϕ is the threshold value of Q; δ is the change in slope past the threshold; and ε is the model error. For those watersheds not exhibiting a strong threshold C-Q response, the above model collapses to a simple linear regression, signified by a near-zero value for δ. The Bayesian framework includes prior knowledge on model parameters (i.e., $\beta_0, \beta_1, \mu, \sigma^2, \phi, \delta$) through the specification of parameter distributions. Vague priors were established for all parameters so that the posterior distributions would be influenced most by the data themselves (Gelman et al., 2004).

2.3.2. Model Diagnostics and Evaluation Criteria

The posterior distributions on the prethreshold (β_1_I) and post-threshold (β_1_II) regression slope parameters for each BLR model run were evaluated as either flat, inclined positively (accretionary), or inclined negatively (dilutionary). If the 95% credible interval (CI) on the posterior distribution of the mean of β_1 included a zero value, the segment slope was deemed flat, or near-zero. The posterior quantiles on the delta (δ) parameter of the model were also examined to determine whether the 95% CI excluded a value of zero. Inclusion of a zero value in the CI for δ would suggest no significant difference between the slopes of Segments I and II, and a simple regression model might equally-well characterize the C-Q relationship. A decision tree for model assignment is included in supporting information Figure S1.

Post hoc analysis of model assignments was performed comparing means of basin characteristics by model type using one-way Analysis of Variance (ANOVA) methods followed by Tukey Honest Significant Differences (HSD) tests between individual group means. For those variables that were not normally distributed (as tested by Shapiro-Wilks method), nonparametric methods were applied (Kruskal-Wallis). Model assignments were also compared on a univariate basis for correlations to physical and hydrological variables, applying Pearson methods (or the nonparametric Spearman's rank method when underlying data were not normally distributed). Statistical tests were performed in JMP (v. 12.0, SAS Institute, Cary, NC).

2.3.3. Model Computation

BLR model fitting and parameter estimation were carried out using Markov-chain Monte Carlo (MCMC) methods. A Gibbs sampler was used to obtain samples from the posterior distribution and estimate the mean, mode, quantiles, and credible intervals for each model parameter. MCMC sampling was implemented in R (R Core Team, 2016) using JAGS (Plummer, 2003) through interfaces developed in software packages, including "rjags" (Plummer, 2016), "runjags" (Denwood, 2016), and "coda" (Plummer et al., 2006). R code for the BLR model is provided in the supporting information. Sampling was conducted with four parallel chains initialized with random number generators, for 100,000 iterations with a thinning factor of 10, after discarding the initial 5,000 iterations for adaptation and burn-in phases. Convergence was confirmed by visual examination of trace plots and the Gelman-Ruben statistic (Gelman & Rubin, 1992); i.e., potential shrink reduction factor less than 1.1. Measures of chain stability and accuracy included Monte-Carlo standard errors (or estimated SD of the sample mean in the chain) and effective sample size (or number of iterations normalized by autocorrelation of chains).

2.4. SOM Model Development

Supporting information Figure S2 contains a conceptual diagram of the SOM used to cluster the study area basins into distinct sediment and nutrient flux regimes based on physical and hydrological variables. Individual observations (vector of input variables, in this case, physical characteristics of the watersheds such as MAP, basin relief, drainage density, etc.) are clustered into output categories (in this case, dominant annual-average sediment or nutrient flux). Details of the SOM algorithm, computational methods, and cluster validation techniques (Vesanto & Alhoniemi, 2000; Vesanto et al., 2000; Wehrens & Buydens, 2007; Anderson, 2001; Oksanen et al., 2017) are provided in supporting information.

The final input data comprise 17 variables, including metrics describing hydrologic, topographic, geologic, and land use characteristics of the 18 tributary basins (Table 1) and selected parameters derived from regressions of C on Q for TSS, PP, and DP. Inputs were range normalized (Alvarez-Guerra et al., 2008) as follows:

$$norm(x_i) = \frac{(x_i - \min(x_i))}{(\max(x_i) - \min(x_i))}.$$

Clusters were examined post hoc for their ability to predict loading, by comparing mean annual TSS/PP/DP concentration, flux, and yield (supporting information Table S2) between clusters. Flux and yield values were log-transformed to ensure normality for application of ANOVA methods. For each input variable, the intracluster mean (on a normalized scale) was plotted against the overall mean, and the magnitude and direction relative to the overall mean was examined to better understand variables driving the clustering.

3. Results and Discussion

3.1. Models of Concentration-Discharge Dynamics Revealed by BLR

BLR methods identified six general C-Q patterns for the LCB watersheds out of the nine classifications proposed by Moatar et al., (2017) (Figure 3a, supporting information Tables S3a, S3b, and S3c). For TSS, the best fit of C-Q data for six of the basins was provided by Model A (i.e., an upward-inclined prethreshold segment, and upward inclined post-threshold segment, or "up-up" pattern), while ten basins exhibited a Model D (flat-up) response and two were classified as Model B (up-flat). Given the close correlation of PP to TSS (average $R^2 = 0.81$; range: 0.50–0.93), model assignments for PP C-Q patterns were nearly identical, with four exceptions. The PP model differed from the TSS model for Mettawee, Little Ausable, and Pike (all D models) and Salmon (A; supporting information Table S3b). A majority of the C-Q responses for DP was classified as Model D (12); additional DP responses were classified as Model G (3), E (2), or C (1), characterized by a down-up, flat-flat, or up-down pattern, respectively.

Our BLR methods permitted the definition of subclasses on the C-Q Model A and I, extending the classification of Moatar et al. (2017) (Figures 3b and 3c). Examination of the posterior for model parameter, δ, allowed us to determine if regression slopes were credibly different before and after the indicated threshold. A steeper post-threshold slope (relative to the prethreshold value) classified the response as either Model A2 (accretionary) or I2 (dilutionary); a lesser post-threshold slope defined Model A3 or I3. In the case of no credible difference between the slopes of Segments I and II (i.e., 95% CI includes zero), the model type was classified as either A1 (accretionary) or I1 (dilutionary). For TSS and PP, respectively, 28% and 22% of our basins were distinguished as having a Model A2 C-Q response.

A degree of uncertainty in model assignment arose in five cases for DP and two for PP. For all model types other than A1, E, and I1, the posterior on the delta (δ) parameter should exclude zero (supporting information Figure S1). However, this was not always the case. For example, the DP C-Q response for Little Otter was assigned to Model D based on a 95% CI for the prethreshold slope that included zero and for the post-threshold slope that excluded zero. However, the 95% CI for δ spanned zero, suggesting no significant difference between the slope values, and that a simple model (A1) could fit the data nearly as well. Similarly, Model A1 could have been substituted for Model D for Poultney (DP), Bouquet (DP), Great Chazy (DP), Pike (PP), and Putnam (PP); and Model E rather than H could have fit the DP data nearly as well for Putnam (Model E rather than H). Several factors may have contributed to this uncertainty. Little Otter and Putnam are small basins that tend to exhibit weaker C-Q correlations (Syvitski et al., 2000). Uncertainty in the DP model assignments may have arisen due to the generally weaker correlation of this solute to Q (i.e., lower β_1 values), as compared to sediment. Finally, in the cases of Poultney and Putnam, representativeness of
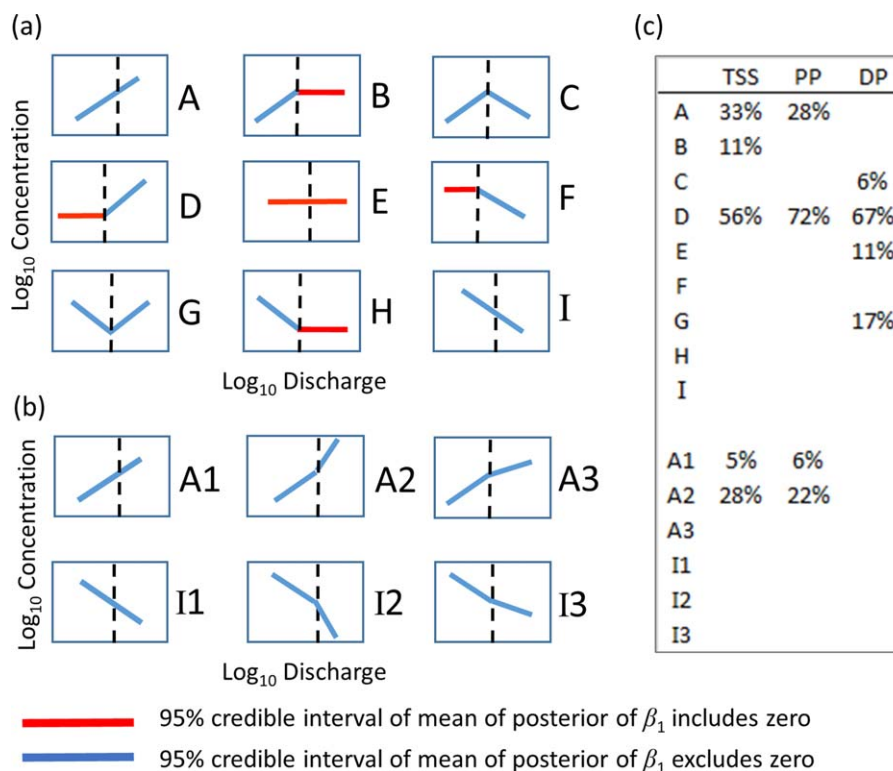
Figure 3. Identification of segmented regression models of $\log_{10}C$-$\log_{10}Q$ relationships, including (a) conceptual models of nine types identified by Moatar et al. (2017), modified to depict a variable threshold position (vertical dashed line), and colored indication of dominant export regime of pre or post-threshold segment: hydrologic (blue) and reactive (red); (b) variations on Models A and I suggested by this study and discerned through examination of posterior distribution of model parameters for BLR; and (c) relative abundance of model types exhibited by study area watersheds for TSS, PP, and DP.

the C-Q time series may have influenced model assignment, as the highest flows are somewhat underrepresented in the available records for these basins (supporting information Table S4).

Overall, the C-Q responses for TSS and PP were dominated by positive slopes including Models A (33 and 28%, respectively) and D (56%, 72%). We attribute this accretionary pattern to the relative abundance of suspended sediments in these post-glacial basins and to legacy stores of phosphorus. A threshold effect in the C-Q response for TSS (and by extension, PP and other sediment associated constituents) is not uncommon (Hicks et al., 2000; Meybeck & Moatar, 2012). A similar distribution of TSS models (62% D and 21% A) was observed by Moatar et al. (2017) in a sampling of 293 gaging stations in French basins ranging from 50 to 110,000 km^2. The C-Q responses for DP in our study area basins were also dominated by positive slopes. Dilutionary effects were relatively uncommon and limited to DP Models C and G for our LCB study area. In this regard, our results differed from those of Moatar et al. (2017), who evaluated a close analog to DP, namely, PO_4^{3-}. The majority of their basins exhibited a stable or declining C trend with Q (Models E, H, or I), while our basin responses were dominated by an accretionary hydrologic response for DP at high flows (67% Model D and 17% G). Our model assignments may not be directly comparable, since we applied Bayesian inference of the 95% CI on the posterior of β_1, and Moatar et al. (2017) used an absolute value of 0.2 for β_1 to distinguish accretionary or dilutionary behavior from a stable response. However, our β_1_II values (mean of posterior distribution) for DP ranged from 0.22 to 0.46, with one exception: 0.13 for Little Otter. Supporting information Figure S3 illustrates pre and post-threshold values for our 18 basins with whiskers denoting the 95% CI on parameter estimates relative to the traditional value of 0.2.

3.1.1. Regression Slopes
3.1.1.1. Prethreshold
For TSS, 10 basins had a flat or nearly flat prethreshold segment (Model D); values of β_1_I for these basins ranged from −0.28 to 0.48 (Figure 4a). However, the 95% CI of the posterior distribution of β_1_I spanned
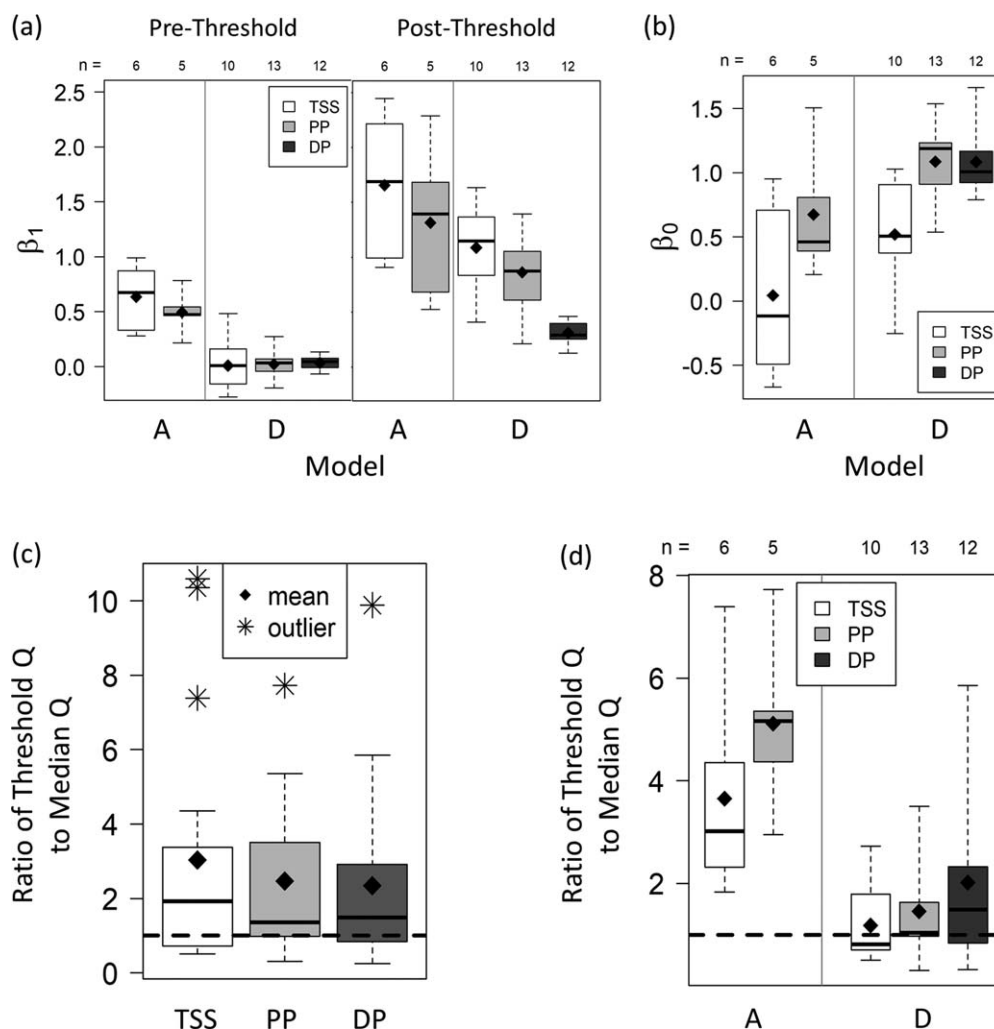
Figure 4. Box plots of: (a) β_1 and (b) β_0 regression parameters by constituent (TSS, PP, and DP) for the most frequently encountered $\log_{10}C$-$\log_{10}Q$ relationships in the Lake Champlain Basin (Models A and D). Letter symbols denote C-Q regression model type after Figure 3. Bottom plots display the ratio of threshold Q to median Q **(c)** by constituent and (d) by constituent for Model types A and D.

zero, suggesting that a zero value is also possible. Six basins exhibited a C-Q pattern with a moderately to strongly inclined prethreshold slope (either Model A1 or A2) with β_1_I values ranging from 0.28 to 0.87, and with the 95% CI on these estimates excluding a zero value. The mean β_1_I value ($\mu = 0.57$) for Model A2 basins was significantly different (ANOVA, $p < 0.05$) and greater than the mean β_1_I value for Model D basins ($\mu = -0.01$). The one Model A1 and two Model B basins had β_1_I values in a range comparable to the Model A2 basins (supporting information Table S3a). Similarly, for PP, the β_1_I values for Model A2 basins ($\mu = 0.42$; range: 0.21–0.54; $n = 4$) were significantly different (ANOVA, $p < 0.05$) and higher than values for Model D basins ($\mu = 0.02$; range: −0.19 to 0.27, $n = 13$). The one Model A1 basin had a β_1_I value comparable to the Model A2 basins. For DP, prethreshold slopes were largely flat or declining. Model D fit a majority of the basins, with β_1_I values ($\mu = 0.03$; range: −0.07 to 0.13; $n = 12$) comparable to those of PP and TSS (Figure 4a).

3.1.1.2. Post-Threshold
For both TSS and PP, the range of values for post-threshold slope, β_1_II, was higher for Model A basins than D basins (Figure 4a). For TSS, the group mean value for Model A2 basins ($\mu = 1.8$; range: 0.99–2.4; $n = 5$) was greater than Model D basins ($\mu = 1.1$; range: 0.41–1.6; $n = 10$; ANOVA, $p < 0.10$). Two Model B basins had statistically significant ($p < 0.10$) lower post-threshold slopes than either A2 or D basins, with β_1_II values of −0.28 and 0.5. For PP, Model A2 basins ($\mu = 1.5$; range: 0.68–2.3; $n = 4$) were greater than Model D

basins ($\mu = 0.86$; range: 0.21–1.4; n = 13; ANOVA; $p < 0.10$). For DP, post-threshold slopes ($\mu = 0.31$; range: 0.13–0.46; n = 12) were less than TSS and PP, although still weakly accretionary. Our Model D values for β_1_II (mean of posterior distribution) ranged from 0.22 to 0.46, with one exception: 0.13 for Little Otter.

3.1.2. Regression Intercepts

Mean values of β_0 were not significantly different between model groups (ANOVA, $p > 0.05$), but PP and DP model intercepts were higher than TSS intercepts (Figure 4b). When considering sediment-related constituents for all 18 basins on a univariate basis (Spearman's rank correlation, $p < 0.10$), the TSS and PP β_0 values correlated negatively to basin relief (–0.469, −0.542) and positively to drainage density (0.511, 0.452). The intercept values for the solute, DP, were negatively correlated to total drainage area, MAP, and basin relief (–0.550, −0.480, −0.689). Additionally, the percent land cover in agricultural use showed a significant positive correlation (0.488) to DP β_0 value. Intercept values for all three constituents (TSS, PP, DP) showed strong positive correlations to mean concentrations of total calcium (0.608, 0.701, 0.641), and mean total calcium (TCa) concentration, itself, was strongly correlated, in a negative sense, to total drainage area (–0.647) and basin relief (–0.845).

Findings for TSS are somewhat inconsistent with some other studies, which identify basin area as a significant factor inversely correlated to the regression intercept for sediment (Nash, 1994; Syvitski et al., 2000). For example, in a study of 57 North American river gaging stations (on 49 rivers) with upstream drainage areas ranging from 720 to 1,680,000 km^2, Syvitski et al. (2000) reported a negative correlation between mean annual discharge (MAQ; as a proxy for basin size) and β_0, with MAQ explaining up to 65% of variance in β_0. With the addition of basin relief, the explained variance in the intercept increased by 5%–70%. Our study found a moderately strong negative correlation to Total Drainage Area (Pearson r = −0.507) for PP, but this relationship was weaker for TSS (r = −0.362). Differences between our results and those of Syvitski et al. (2000) may be related to the wide range of basin sizes examined in the latter study. If their data set is restricted to basins of comparable size (i.e., less than 5,000 km^2, n = 11), a similar negative correlation value is obtained (r = −0.413). Notably, all the intercept values calculated by Syvitski et al. (2000) were less than zero, while our intercept values included a mix of positive and negative values. Syvitski et al. (2000) values were based on simple linear regressions, which may underestimate the β_0 value in threshold-affected watersheds. Employing segmented regressions has allowed for a less constrained interpretation of β_0 relative to other basin variables, wherein the β_0 value is less tied to the magnitude of β_1. In other words, under the constraint of simple linear regression, an increase in β_1 will necessarily be associated with a decrease in β_0 (Asselman, 2000; Warrick, 2014). Under a segmented model fit, the magnitude of β_0 is less constrained by collinearity with the post-threshold slope, β_1_II (see Figure 1), and thus more useful for characterizing export dynamics.

3.1.3. Threshold Magnitude and Frequency

Model types were further reviewed for differences in threshold magnitude and frequency by examining the threshold value expressed as a ratio to the median Q (supporting information Tables S3a, S3b, and S3c) and computing the percentage of time that the threshold is exceeded. Notably, threshold positions identified for TSS/PP/DP models by our BLR methods, demonstrated a considerable range below and above the median Q (Figure 4c). The threshold position expressed as a ratio to the median Q was particularly high for two TSS Model B basins, one TSS Model A2 basin, PP Model A1, and DP Model E (comprising the outliers in Figure 4c).

The 10 TSS Model D basins ($\mu = 1.2$; 0.5–2.7) generally had lower threshold positions than Model A2 basins ($\mu = 4.0$; 2.3–7.4; Figure 4d) and group means were statistically different (Wilcoxon rank-sum, $p < 0.05$). Consequently, the percentage of time that the TSS threshold was exceeded was greater for Model D basins (17–72%) than for Model A2 basins (2–20%), (Wilcoxon, $p < 0.05$). Thus, D basins are spending a relatively large amount of time in a functional stage characterized by positive C-Q correlation. The one A1 basin had a threshold position similar to the A2 basins. Two Model B basins (Little Ausable and Salmon) had very high threshold positions, exceeded less than 2% of the time, beyond which C-Q data transitioned from a positive correlation to a flat response. The PP C-Q response reflected a similar pattern, with Model D basins exhibiting significantly lower threshold positions than Model A2 basins. No significant difference between DP models was observed for threshold ratios, which ranged widely from 0.2 to 9.9 times the median Q. DP Model D basins had a similar central tendency and range of threshold ratio as their TSS and PP counterparts (supporting information Figure S3b).

On a univariate basis, the TSS and PP threshold ratios were positively correlated to the slope of the prethreshold segment (0.712, 0.571, Wilcoxon, $p < 0.05$), since Model A2 basins (with higher threshold positions) are characterized by inclined prethreshold slopes while Model D basins (with lower threshold positions) have near-flat prethreshold slopes. DP threshold ratios were positively correlated to the post-threshold regression slope—a reflection of the fact that a majority of those basins with thresholds above the median Q were classified as either Model D or G, which demonstrate a positive C-Q relationship for the post-threshold segment.

3.1.4. Sediment and Solute Export Regimes

Regression and variance metrics can be used to classify sediment and nutrient export regimes of catchments on a continuum from chemodynamic to chemostatic, and from positive to negative correlation of the log C-Q relationship. We have adapted the bivariate plot of β_1 and CV ratio suggested by Musolff et al. (2015) as a convenient way to compare our results to theirs, and to highlight the advantages of a segmented regression model for discerning variable export regimes for pre and post-threshold flow stages. Musolff et al. (2015) identified two overlapping zones for chemodynamic response of TSS and total phosphates, denoting export regimes dominated by "threshold-driven" and "reactive" processes, with the latter straddling the $\beta_1 = 0$ line (Figure 5a). Their conceptual model defined "threshold-driven" responses as being
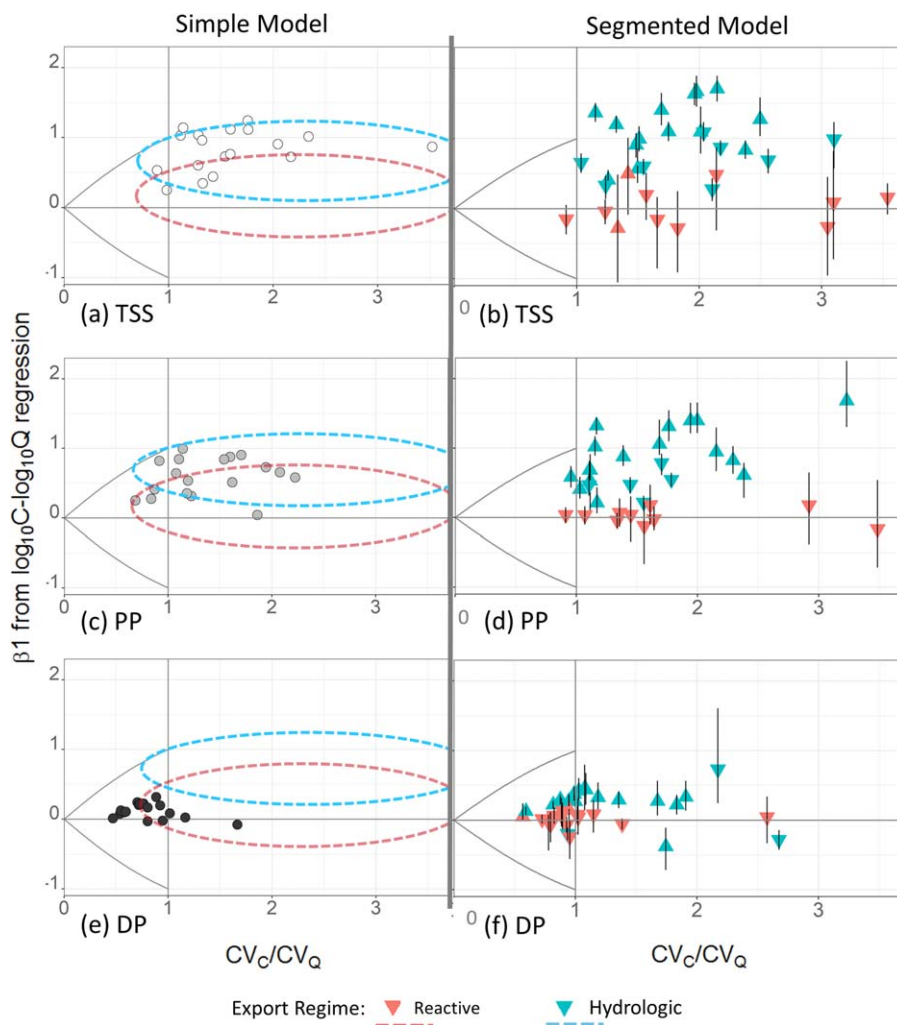

Figure 5. Plot of regression slope (β_1) versus CV ratio to visualize export regime for (top plots) TSS, (middle) PP, and (bottom) DP from 18 LCB watersheds, respectively, (using presentation style of Musolff et al., 2015). Simple regression data are presented in Figures 5a, 5c, and 5e; segmented regression data are presented in Figures 5b, 5d, and 5f, with metrics for prethreshold data (down-directed triangle) plotted separately from post-threshold data (up-directed triangle). Vertical whiskers span the 95% credible intervals around the estimate of β_1 defined by BLR. Bounds in the top left and bottom left of each plot are defined solely by CV_Q and β_1 (not CV_C), and have been derived from the mean and standard deviation of Q from Bouquet data (see Musolff et al., 2015 for further discussion).

episodic in nature with a strongly positive relationship between C and Q (i.e., high β_1 value). These are systems in which C variability is driven predominantly by Q variability, and both Musolff et al. (2015) and Thompson et al. (2011) mapped TSS to this category. To avoid confusion, and for consistency with Moatar et al. (2017), we have used a more generalized term—"hydrologic"-ally driven (Figure 5)—for rivers that plot to this zone, since use of the term "threshold-driven" by Musolff et al. (2015) does not appear to suggest a prerequisite that all watersheds of this zone exhibit a distinct threshold(s) in the C-Q pattern. For example, a Model A, E, or I response could plot to this zone. In contrast, "reactive" responses reflect processes that are more independent of fluctuating Q and that are characterized by rapid in-stream cycling (Musolff et al., 2015). Musolff et al. (2015) and Thompson et al. (2011) identified ammonium and phosphates in this category, citing the importance of biologically and chemically mediated processes in controlling C. Similarly, Moatar et al. (2017) identified a weak C-Q relationship ("reactive" response) for TSS at flows below the median Q, and suggested the importance of biochemical processes in regulating TSS concentration at these low-flow stages. In the context of sediment and sediment-related constituents, we expand the definition of "reactive" export regimes to include the array of biologically, chemically, and physically mediated processes that are responsible for the removal (uptake) or return (release) of constituents from advective transport (Fisher et al., 1998). Thus, for PP and TSS, "reactive" could include nonchemical and nonbiological processes that are largely decoupled from Q, such as lateral and vertical exchanges of fine sediment and associated constituents between the water column and the stream bed, channel margin deposits, disconnected flood chutes, or floodplain (Boano et al., 2014; Karwan & Saiers, 2009; Skalak & Pizzuto, 2010).

Figure 5 illustrates bivariate plots for TSS, PP, and DP from our 18 LCB tributaries based on simple linear regression (Figures 5a, 5c, and 5e) and segmented regression (Figures 5b, 5d, and 5f). Overall, a stronger C-Q relationship is suggested by data points derived from a segmented regression than is revealed by the simple regression results (supporting information Text S3), leading to greater dispersion on the β_1/CV ratio plot. (Select data points with very high β_1 or CV values plot off the chart and are not represented in Figure 5 for image clarity). For TSS and PP, post-threshold data generally have higher, positive β_1 values and thus plot above the prethreshold points, which tend to assemble close to the horizontal line marking a zero value for β_1. In the case of DP, the points assemble closer to the zero line, reflecting the generally lower β_1 values for this solute.

Figures 5b, 5d, and 5f also help visualize the uncertainty on the pre and post-threshold β_1 parameter explicitly estimated from our BLR approach, and how this was leveraged to classify model types (Figures 3a and 3b) as well as assign a "reactive" or "hydrologic"-ally driven export regime (Musolff et al., 2015). The posterior distribution of the β_1_I (or β_1_II) parameter available from the BLR was examined, and if the 95% CI spanned a value of zero, the point was classified as "reactive" and color-coded red. Otherwise, the point was classified as "hydrologic"-ally driven and coded blue.

For TSS and PP, the C-Q relationship of the prethreshold stage in some cases plots to the "reactive" zone, rather than the "hydrologically-driven" zone (i.e., the Model D basins). During the low-flow functional stage, C dynamics are nearly independent from Q (i.e., r^2 values for logC-logQ regressions are very low); and therefore, β_1 metrics provide minimal information for interpretation (Thompson et al., 2011). These basins are distinguished from the Model A1 and A2 basins in which the prethreshold points were classified as "hydrologic"-ally driven (color-coded blue) and β_1 values defined some credibly positive slope, ranging on a continuum from modestly to substantially accretionary. For TSS, two basins exhibited a "reactive" post-threshold slope (Model B). For both basins (Salmon and Little Ausable), the indicated threshold is high (greater than 10 times the median Q), and the pattern may reflect particle exhaustion at these highest discharges. In the case of Little Ausable, the apparent C-Q pattern may also be a function of having poor sample representation from these highest flow ranges (supporting information Table S4). For DP, a majority of the prethreshold stages were classified as "reactive" (Models D or E); a few basins demonstrated a hydrologically driven response at low flows—either accretionary (Model C) or dilutionary (Model G). Similarly, most basins exhibited a hydrologically driven post-threshold response (Model D or G), although a few were either dilutionary (Model C) or stable (Model E). Two basins have a pre or post-threshold value that is negative and greater in absolute value than 0.2 (Otter Model C and Little Chazy Model G).

Previous researchers (Basu et al., 2010; Musolff et al., 2015; Thompson et al., 2011) have suggested an absolute value of 0.2 for the regression slope as a "cut-off" to distinguish between reactive and hydrologic response. Bayesian inference provides an alternative, data-driven approach for interpretation of the

regression slope parameter, which also offers insight into the uncertainty of model assignment. Interestingly, most of our model assignments employing BLR conformed to this rule of thumb, with accretionary or dilutionary responses defined by a mean of the posterior on $\beta 1$ values $> |0.2|$. Generally speaking, the uncertainty of the β_1 estimate, or length of whiskers defined by the Bayesian credible interval, is greater in magnitude for the prethreshold slopes than the post-threshold slopes for all three constituents. This finding may reflect seasonal shifts in "reactive" versus "hydrologic" process dominance at these low flows, as moderated by factors such as temperature, plant growth, and aquatic biota. For example, recent research, aided by high-frequency sampling, suggests that the transition between functional stages is dynamic and driven largely by meteorological variables such as antecedent moisture or rainfall intensity, rather than being predominantly a function of basin-scale physical features (Bende-Michl et al., 2013; Bieroza & Heathwaite, 2015). Additionally, interannual shifts in threshold position may be contributing to uncertainty in the β_1 estimate (e.g., due to river system responses to extreme events, changing land use patterns or progressive implementation of watershed restoration projects, and best management practices) (Zhang et al., 2016).

Thus, while previous research has suggested that TSS and PP C-Q patterns are consistently hydrologically driven at a basin scale (Musolff et al., 2015), our BLR approach suggests that TSS and PP export regimes can exhibit more complexity. In some threshold-affected systems, low discharge ranges may comprise a distinct functional stage that is more dominated by reactive processes, including and facilitated by lateral and vertical exchanges of fine sediment within the hyporheic and parafluvial zones which temporarily remove constituents from advective flow. In this context, the river corridor can be viewed as a reactor facilitating changes in particulate P concentration, as opposed to just a vessel for transport (Harvey & Gooseff, 2015; Mulholland et al., 1997; Withers & Jarvie, 2008).

The variance in threshold position among watersheds is a reflection of the duration of time that each watershed stays in a particular functional stage of sediment/nutrient flux. For example, although not a focus of this current study, the seasonal distribution of flows that exceed the PP threshold may influence the relative annual flux among basins. A cursory review of 1990–2015 discharge data indicates that the PP Model D basins spend a majority of their time ($>50\%$) in the prethreshold, reactive, functional stage during the months of June through October (supporting information Figure S5). Most of the basins are also dominantly in this reactive functional stage during the month of February (all except Poultney). Some of the Model D basins (Great Chazy, Little Otter, Mettawee, and Winooski) spend a majority of all months except April in this reactive functional stage; these are basins with a particularly elevated threshold position exceeded between 13 and 29% of the time on an annual basis. The latter three basins have some of the highest mean annual concentrations of PP (supporting information Table S2). Future application of our novel approach will examine seasonal variation in threshold position and functional stages of nutrient and sediment export.

3.2. SOM Clustering of Watersheds for PP and DP

By preclassifying our eighteen LCB tributaries into distinct C-Q patterns, relying on Bayesian inference, we have improved the utility of regression metrics to suggest between-watershed differences in drivers and capacity for system export of sediment and phosphorus. This expanded set of regression metrics can be included, alongside other basin metrics, as inputs to a SOM for grouping our humid temperate basins by constituent export regime. Our main intent was to discern whether the combination of watershed characteristics and export regime was responsible for greater or lesser flux of PP and DP to Lake Champlain. For example, it is conceivable that a basin that exhibits a strong sediment/PP C-Q response but has low overall P source strength due to land cover patterns, may generate low overall flux to LCB. Conversely, a basin with high sediment and P source strength may generate low flux to LCB if there are aspects of topography, climate, or geomorphic setting that enhance storage or attenuation of sediment/PP within the river network leading to a weaker C-Q response (i.e., lower β_1). Therefore, we included both watershed characteristics (i.e., precipitation, discharge, soils, land cover, etc.) and export regime metrics as inputs to a PP SOM and DP SOM, in order to model these nonlinear, epistatic relationships, and cluster the basins by overall average annual flux of TSS and PP to Lake Champlain.

For each constituent, the 18 basins were assigned to three distinct clusters and multivariate input data (Table 1 and supporting information Tables S3a–S3c) have been reduced to a 2-D lattice for visualization: a 3×6 lattice for PP (Figure 6a) and a 4×4 lattice for DP (Figure 7a). The column-to-row ratio for theses lattices approximated the ratio of the first two principal components of the input data (5.7/3.4 for PP; 4.3/3.2 for
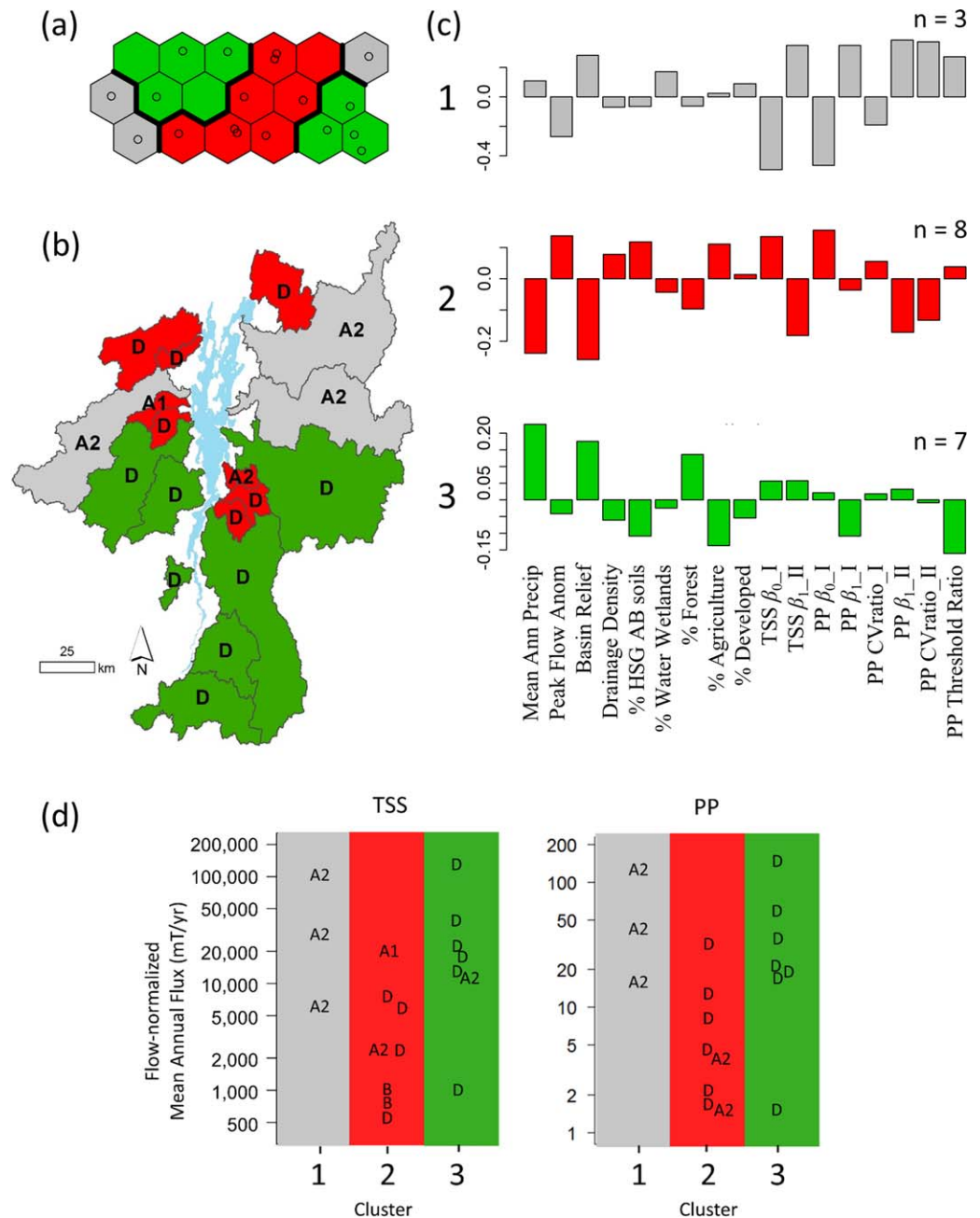
Figure 6. Particulate phosphorus SOM clustering outcomes for Lake Champlain Basin tributaries, including (a) SOM lattice (see supporting information Figure S2 and Text S2); (b) basin location map color-coded by SOM cluster assignment and keyed to C-Q regression model types; (c) variable bar plots by cluster (n = number of basins per cluster; y axis represents range-normalized values; refer to section 2.4). Note: for clarity of presentation, variable plots have been rendered using different vertical scales. (d) Mean annual flux of (left) TSS and (right) PP in metric tons per year (mT/yr) by SOM cluster. Color shading relates to clusters in Figures 6a–6c. Letter symbols denote C-Q regression model type after Figure 3. Flux estimates are from Medalie (2014).

DP; PCA on correlations), as per Cereghino and Park (2009). Clustering outcomes were slightly different for each constituent (Figures 6b and 7b), driven by differing combinations of input variables (Figures 6c and 7c).

3.2.1. PP SOM Results

ANOVAs revealed significant differences between mean cluster values for flow-normalized flux of both TSS and PP ($p < 0.10$; Figure 6d), but not for mean annual concentration or yield ($p > 0.10$). Post hoc testing applying Tukey HSD showed that the mean flux values for Clusters 1 and 3 were higher than, and
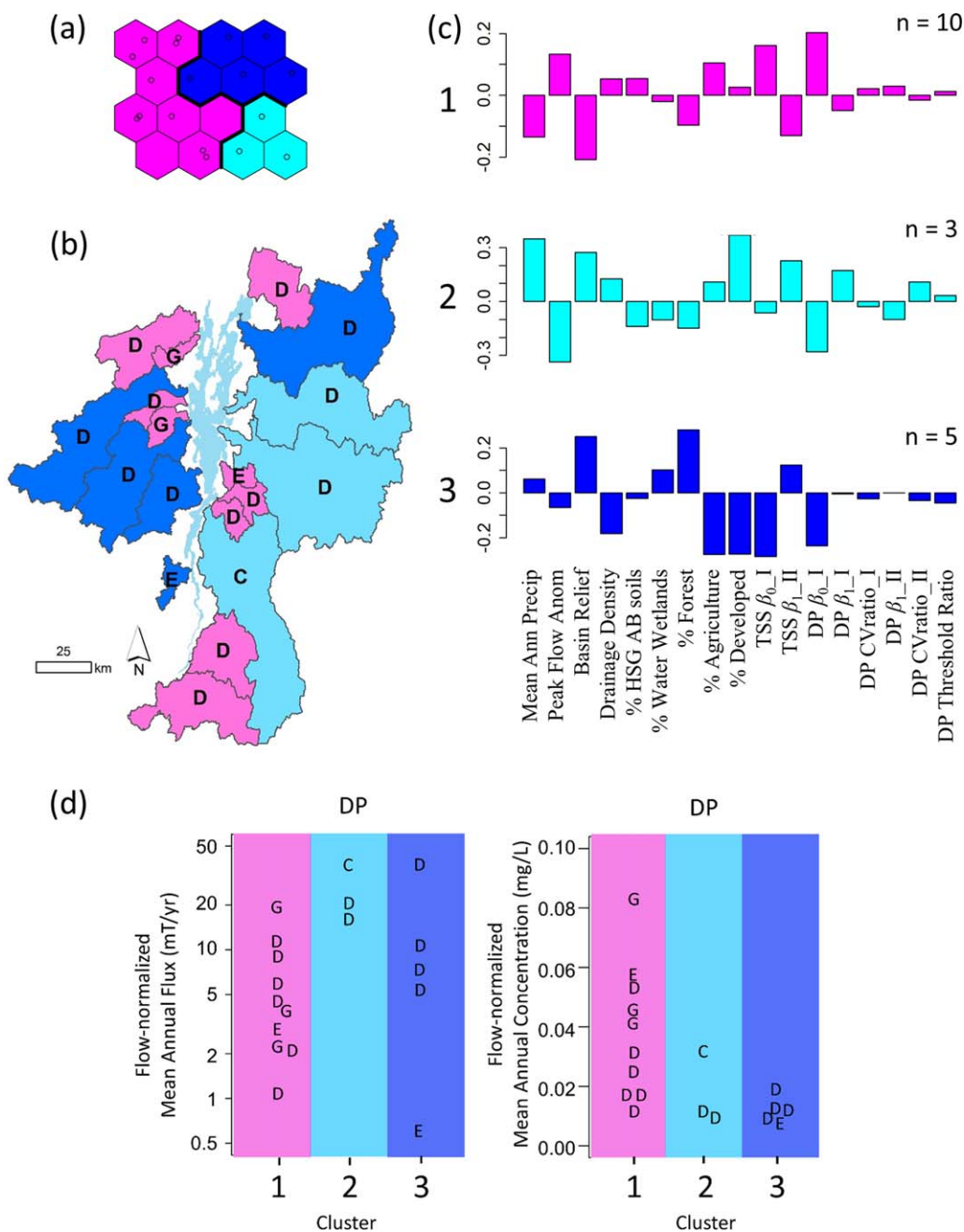
Figure 7. Dissolved phosphorus SOM clustering outcomes for Lake Champlain Basin tributaries, including (a) SOM lattice; (b) basin location map color-coded by SOM cluster assignment and keyed to C-Q regression model types; (c) variable bar plots by cluster (n = number of basins per cluster; y axis represents range-normalized values; refer to section 2.4). Note: for clarity of presentation, variable plots have been rendered using different vertical scales. (d; left) Mean annual flux in metric tons per year and (right) concentration in milligrams per liter of DP by SOM cluster. Color shading relates to clusters in Figures 7a–7c. Letter symbols denote C-Q regression model type after Figure 3. Flux and concentration estimates are from Medalie (2014).

statistically different from, Cluster 2 for both PP and TSS ($p < 0.10$). Larger basin sizes were generally associated with greater flux of TSS and PP. However, Clusters 1 and 3 comprised basins of similar size, but clustered separately.

3.2.1.1. Higher-Flux Basins of PP Clusters 1 and 3

Cluster 1 and 3 basins each exhibit strong threshold effects in the C-Q response for both TSS and PP: Model A2 for Cluster 1 and Model D for Cluster 3, except Mettawee in Cluster 3, which was classified as Model A2

for TSS. While both Cluster 1 and 3 basins demonstrated higher-than-average flux of PP and TSS (Figure 6d), a different combination of variables appears to be driving this pattern in each case (Figure 6c). These two clusters share some variables in common—including, higher-than-average values for basin relief and MAP.

Variables that distinguish these two higher-loading Clusters (1 and 3) from each other (i.e., variables that trend in opposite directions from the overall mean) include the regression intercepts for both TSS and PP and the post-threshold response for PP (Figure 6c). Cluster 1 (Model A2) basins appear to have greater transport capacity (larger β_1_II values) relative to Cluster 3 (mostly Model D) basins (Figure 4d). However, threshold position as a ratio to the median Q was higher for Cluster 1 than 3 basins, although not significantly so (ANOVA/Tukey HDS, $p > 0.10$). This would mean that transport of sediment and sediment-bound P occurs disproportionately during less-frequent, higher-magnitude flows in these Model A2 basins—i.e., they exhibit a more episodic C-Q response than Model D basins, and could be considered supply limited with respect to TSS and PP (Basu et al., 2011; Thompson et al., 2011). Importantly, Model A2 basins also have steeper prethreshold slopes relative to Model D basins. Therefore, small discharge events are more impactful on TSS and PP export than similar magnitude events in Model D basins.

Cluster 1 basins appear to have a much lower range of β_0 values for each constituent than their Cluster 3 counterparts, reflecting a lower baseline supply of suspended sediment and particle-bound P in the former group. The lower-than-average β_0 values for TSS and PP (as well as the higher-than-average β_1 values previously noted) in Cluster 1 basins (Saranac, Lamoille, and Missisquoi) may also be related to in-stream impoundments (supporting information Table S1) and the possible storage of fine sediments and PP behind dams at least during low to moderate flow stages. For example, Wang et al. (2008) noted a stepped decrease in the intercept parameter for C-Q regressions developed for TSS time series data on the Yangtze River in China, as in-stream impoundments were constructed to support generation of hydropower. At the same time, they attributed observed increases in β_1 to the increased erosive power in the lower reaches of the Yangtze River in China, resulting when upstream impoundments sequestered sediments and led to decreased downstream concentrations of suspended sediments (so-called, "hungry water" effects of Kondolf, 1997). Elevated β_1 values in impounded rivers have also been attributed to effects of diminished sediment storage capacity of in-stream reservoirs (Zhang et al., 2016).

Cluster 3 basins tend to be dominated by lower-infiltration soils (exhibit lower percentages of HSG A and B soils). This is likely a reflection of their geographic position with near-lake areas located in the Champlain Valley or Vermont Valley/Taconic biophysical regions. These regions are associated with silt and clay deposits from postglacial freshwater and brackish-water lake episodes that inundated the valley to higher stages than the present Lake Champlain (Stewart & MacClintock, 1969). Similarly, Medalie (2013) noted a significant correlation between physiographic province and both concentration (Kruskal-Wallis $p = 0.092$) and flux ($p = 0.045$) of total phosphorus. This difference between Cluster 1 and Cluster 3 basins is particularly illustrated when comparing the Winooski basin (Cluster 3) to Lamoille and Missisquoi basins (Cluster 1). Despite similar size, relief, MAP, and impoundment/flow regulation status, these basins clustered differently for PP, driven in large part by differences in β_0 values which resulted in their assignment to different regression model types (e.g., Winooski, TSS_ $\beta_0 = +0.37$, Model D versus Lamoille and Missisquoi values of -0.67 and -0.29, Model A2). This higher-than-average baseline supply of sediment (and PP) for Winooski basin, could reflect the fact that, on a basin scale, Winooski has a somewhat greater dominance of lower-infiltration soils (lower percentage of HSG A and B soils) than Lamoille or Missiqoi (Table 1). This pattern may also reflect differential source regions and connectivity of PP and TSS (Doyle et al., 2005) and may be a function of between-watershed differences in the dominant geomorphic state of the channel (aggradational versus incisional) (Kline & Cahoon, 2010; Roy & Sinha, 2014) and duration of recovery time for vegetative boundary conditions following extreme flood events (Wolman & Gerson, 1978).

Post-threshold CV ratios for PP (and TSS) were elevated in Cluster 1 basins relative to the average for each of the other clusters. This pattern hints at the importance of less frequent, higher-magnitude storms in producing suspended sediment, and sediment-bound P in these basins. Also, in our study area, impounded and/or regulated rivers did tend to have lower CV_Q values than nonregulated rivers (Wilcoxon, $p < 0.10$), which would contribute to somewhat elevated CV ratios for both TSS and PP, and further promote the

importance of low-frequency, higher-magnitude storms for sediment, and sediment-bound P export (Meade, 1982).

3.2.1.2. Lower-Flux Basins of PP Cluster 2

Cluster 2 basins had lower flux of TSS and PP than Clusters 1 and 3 (Figure 6d). Cluster 2 basins are generally smaller in size (137–778 km^2) with C-Q relationships representing a mix of Model types (A1, A2, B, and D). They have higher background supplies of TSS and PP (elevated β_0 values), and are generally of lower relief with lower MAP. Mean values for relief and MAP are significantly different (ANOVA, $p < 0.05$) and lower for Cluster 2 than Cluster 1 (and 3). Cluster 2 basins exhibit lower-than-average post-threshold β_1 values for both TSS and PP, perhaps related to lesser stream power that would be expected from the combination of smaller basin size, lower relief, and lesser MAP. Cluster 2 basins are also characterized by less-than-average forest cover and somewhat greater-than-average percentage of agricultural land use (although land use is not a significant factor driving clustering). Interestingly, while Cluster 2 basins overall contribute smaller loads of TSS and PP than Cluster 1 or 3 basins (likely related to their smaller size), they are characterized by a mean annual PP concentration range that is higher than that of the Cluster 1 basins (though the overall cluster means are not significantly different at $\alpha = 0.10$) and statistically different than mean PP concentration for Cluster 3 (ANOVA, $p < 0.05$). This result may be due to the fact that even at low flow ranges, these basins have sufficient power to entrain and mobilize fine particles and associated P from legacy stores (i.e., elevated β_0 values) derived from the erodible glaciolacustrine soils and sediments of the Champlain Valley.

3.2.2. DP SOM Results

The DP SOM also clustered basins into three groups, but the group composition varied somewhat from that generated by the PP SOM (Figure 7). Log-transformed DP (and TSS) flux values for Clusters 2 and 3 were higher than Cluster 1, although statistically significant only between groups 2 and 1 (ANOVA/Tukey HSD, $p < 0.10$). Notably, these are nearly the same basins that comprised the high-flux clusters for PP, with the exception of Poultney and Mettawee (compare Figures 6 and 7). In contrast, DP concentrations were higher for Cluster 1 than Clusters 2 and 3, and the means between Clusters 1 and 3 were significantly different ($p < 0.05$) (Figure 7d). There were no significant differences between mean cluster values for DP yield ($p > 0.10$).

3.2.2.1. Higher-Flux Basins of DP Clusters 2 and 3

The higher-flux basins of Clusters 2 and 3 tended to have higher-than-average basin relief and MAP, which can be attributed in part to their larger total drainage area (Figure 7b). Cluster 2 basins were larger than Cluster 3 basins, which themselves were larger than Cluster 1 basins, and the difference between group means was statistically significant (ANOVA/Tukey HSD, $p < 0.05$). Basins in Clusters 2 and 3 also tended to have lower than average regression intercept values, suggesting lower baseline supplies of DP. Interestingly, they also exhibited higher values for the slope parameter on the post-threshold segment of the TSS C-Q regression. This may reflect enhanced sediment transport capacity of these basins, given their higher-than-average relief, which itself is correlated to greater MAP (Pearson r = 0.480 for all 18 basins). To some degree, elevated β_1_II values may also reflect greater availability of TSS sources (e.g., enhanced floodplain connection) at higher flow stages (Asselman, 2000). We speculate that higher availability of TSS could lead to reduced DP flux as a result of sorption (i.e., nutrient cycling).

Land use appears to contribute to differences between higher-flux Clusters 2 and 3 and suggests alternate sources of DP. Cluster 2 basins tended to be more developed and less forested, while the opposite was true for Cluster 3 basins, and the difference between cluster means was significant in each case ($p < 0.10$ for forested, $p < 0.01$ for developed). Cluster 2 basins (Otter, Winooski, and Lamoille) include the urban centers of greater Burlington, Montpelier, Rutland, and Middlebury, which are serviced by wastewater treatment facilities. The mean value of post-threshold regression slopes for Cluster 2 basins is greater than Cluster 1 basins, though not significant ($p = 0.18$), suggesting a more hydrologically driven transport of DP for these basins.

3.2.2.2. Lower-Flux Basins of DP Cluster 1

The lower-flux basins of DP Cluster 1 are characterized by lower-than-average relief and MAP. In contrast to the other basins, they have elevated β_0 values for both TSS and DP, indicating higher baseline supplies of these constituents. Higher DP β_0 values may also be a reflection of the higher-than-average agricultural land use in Cluster 1 basins. Although it was not an input to the SOM, the mean concentration of total calcium (TCa) appears to have been a latent variable driving clustering of basins for DP. Cluster 1 had significantly higher mean TCa than Cluster 2 and 3 basins (ANOVA/Tukey HSD, $p < 0.05$). Elevated TCa concentrations and TSS β_0 values for TSS in Cluster 1 basins may both be a reflection of their geographic

position within the Champlain Valley or Vermont Valley/Taconic biophysical regions, characterized by carbonate bedrock and erodible glaciolacustrine sediments. Thus, DP in these Cluster 1 basins may be attenuated through sorption to, or biogenic coprecipitation with, calcite-bearing particles (Moatar et al., 2017). While Cluster 1 basins are responsible for generally lower flux of DP to Lake Champlain (due largely to their smaller size), they do however, exhibit higher DP concentrations than either Cluster 2 or 3 basins (Figure 7d).

3.2.3. Sediment and Solute Export Regimes Revealed by SOM Clustering

Nonparametric SOM clustering results suggest that different functional stages of C-Q are responsible for the flux of sediment and nutrients to Lake Champlain from different basins. For TSS and PP, two unique clusters of high-flux basins were identified. In the first group, sediment and sediment-bound P flux is hydrologically driven and disproportionately occurring during relatively infrequent, high-magnitude runoff events. During hydrologically and hydraulically dominated functional stages, TSS and PP are entrained and mobilized as a result of stream bed scour, stream bank collapse, rill erosion, gully formation, floodplain scour (where hydrologically connected), and mass movement of strath terraces or closely coupled hillsides (Baker, 1977; Benda & Dunne, 1997; Nanson, 1986; Trimble, 1997; Walling et al., 1999; Walling & He, 1999; Yellen et al., 2014). In the stream channel, sediment and solute transport would be more dominated by advective forces in a downstream direction than by diffusive or dispersive forces in either a lateral or vertical direction (Ward, 1989). Accretionary and hydrologically dominated patterns may also result from progressive or sudden release of sediments from in-stream impoundments at high flows (Meade, 1982; Wang et al., 2008). The inclined pre and post-threshold stages of these Model A2 watersheds may reflect suspended sediments liberated from a two-phase bed load transport regime where sediments accumulated in the channel between storm events are more readily moved, while the second phase consists of additional fines liberated from disturbance of a coarse streambed armor layer (Jackson & Beschta, 1982; Reid et al., 1997; Ryan et al. 2002), or as stabilizing biofilms or aquatic vegetation are breached (Lawler et al., 2006). Alternatively, this pattern may simply reflect expansion of the variable source area with increasing stage (Asselman, 2000; Dunne & Black, 1970).

In the second group, the sourcing and mobilization of sediment and P are more bimodal, resulting from both hydrologic processes at post-threshold discharges and reactive processes (such as nutrient cycling or lateral/vertical exchanges of fine sediment) that dominate at prethreshold discharges. For these basins exhibiting a "reactive" export regime in prethreshold flow stages (i.e., near-flat trends in C with increasing Q), the vertical and lateral components of flow appear to gain influence relative to longitudinal (i.e., downstream) components. This may be due, in part, to lesser overall magnitudes of discharge, but may also reflect different hydrogeomorphic patterns in these rivers (i.e., an enhanced degree of floodplain connection, greater diversity of channel and bed forms, greater percentage of in-stream storage from impoundments or channel-contiguous wetlands than their "hydrologically-driven" counterparts). Research suggests that biogeochemical and physical processes other than advection dominate these reactive functional stages, such as: hyporheic exchange (Karwan & Saiers, 2009); vertical exchange or filtering (Boano et al., 2014); lateral exchange with fine-grained channel margin deposits (Skalak & Pizzuto, 2010; Withers & Jarvie, 2008); microscale bed form migration (Harvey et al., 2012; Pizzuto, 2014); and attenuation in in-stream wetlands (e.g., Qian & Richardson, 1997), impoundments (Wang et al., 2008), or transient storage areas behind large woody debris jams (Wohl & Beckman, 2014). Lagged groundwater recharge from antecedent storms (Bieroza & Heathwaite, 2015) may cause short-term dilutionary effects that contribute to variability in prethreshold TSS and PP C patterns. It is also possible that some of the more elevated concentrations result, not from reactive processes, but from hydrologically driven sediment transport when the turbidity measured at the basin outlet has been generated by localized storms from distal areas of the basin (Bieroza & Heathwaite, 2015; Lawler et al., 2006). We speculate that this reactive functional stage of sediment/nutrient flux could also include bioturbation by wildlife (e.g., beavers and benthic organisms) as cited in Boano et al., (2014) and humans (e.g., active ditching of first-order streams that deliver suspended sediments during low-flow time periods), based on direct observations from these basins.

DP export to Lake Champlain from high-flux basins appears to result largely from a mix of hydrologic processes at post-threshold discharges and reactive processes (nutrient cycling) at prethreshold discharges. Hydrologic phases of transport appear to be dominantly accretionary in nature. This result contrasts somewhat with findings of Moatar et al., (2017) who noted chemostatic or dilutionary responses in a majority of their study basins. The accretionary response in our study area may reflect sourcing and mobilization of DP: (1) from impoundments at high flow stages; (2) from wastewater treatment facilities or combined sewer

outflows at higher discharges; (3) from increased connections to channel-contiguous wetlands at higher flow stages (Watson et al., 2016); or (4) from tile drainage systems (Franzi et al., 2009). Two high-flux DP clusters appear to be distinguished by basin-scale land use, with developed uses associated to one cluster, and agricultural uses more prevalent in the other. Still, post-threshold β_1 values for DP are generally much lower than β_1 values for PP (Figure 4a). This observation is also reflected in the lower overall flux estimates for DP as compared to PP (i.e., compare Figure 6d to 7d).

4. Conclusions and Implications

We have outlined a methodological approach to expand upon previous classification schemes for sediment and solute export from catchments (Moatar et al., 2017; Musolff et al., 2015; Thompson et al., 2011; Zhang et al., 2016), with a focus on suspended solids and particulate and dissolved phosphorus. Using the Lake Champlain Basin to examine concentration-discharge dynamics, our method leveraged information from Bayesian inference to achieve estimation of segmented regression model parameters, and identify threshold position to avoid potential bias in manual threshold selection. Notably, threshold positions identified by our BLR methods, demonstrated a considerable range below and above the median Q – which has been used by previous researchers (Meybeck & Moatar, 2012; Moatar et al., 2017) as a default break-point to classify segmented C-Q regression models and discern differences between pre and post-threshold export regimes. The BLR approach identified different functional stages of TSS, PP and DP export, in that a probability distribution on pre and post-threshold regression slopes from a segmented regression model could be interpreted to discern between "reactive" and "hydrologically-driven" stages of constituent export. We extended the term "reactive" export regime to include the array of biologically, chemically, and physically mediated processes that are responsible for the uptake or release of constituents from advective transport.

Additionally, this study has applied a nonparametric clustering and data visualization approach, using an SOM, to yield insights into nonlinear combinations of independent variables that appear to be driving basin-scale differences in mean annual flux and concentration of sediment and phosphorus. Though further testing with greater numbers of basins would be useful, the SOM results helped define two unique clusters of high-flux basins for TSS and PP. In the first group, sediment and sediment-bound P flux is hydrologically driven and disproportionately occurring during relatively infrequent, high-magnitude runoff events. In the second group, the sourcing and mobilization of sediment and P are more bimodal, resulting from both hydrologic processes at post-threshold discharges and reactive processes (such as nutrient cycling or lateral/vertical exchanges of fine sediment) that dominate at prethreshold discharges. The former functional stage generates an acute flux response and may be more consequential in the context of loading to the lake (e.g., TMDLs and sediment budgets). However, the latter functional stage generates a more chronic concentration response that may be of greater concern in the context of ecological balance in the receiving waters (Bende-Michl et al., 2013). For example, in a hydrodynamically and ecologically diverse receiving water like Lake Champlain (Xu et al., 2015a, 2015b), understanding and predicting the magnitude, timing, and location of these episodic versus chronic inputs of nutrients is critical to projecting riverine load impacts on lake water quality and ecosystems across both time and space (Giles et al., 2016; Isles et al., 2017). Shallow segments of the lake, where P availability and ecosystem productivity are most impacted by benthic P loading (Isles et al., 2015), large PP loads from episodic high-flow events can remain potentially bioavailable for years to decades; but chronic inputs will also accumulate over time and persist in these environments (Isles et al., 2017, Zia et al., 2016). Deeper sections of the lake could be more impacted by chronic inputs of DP, as even during large events, particulate phosphorus quickly settles to depths where it is no longer potentially bioavailable to phytoplankton, and the short-term (days to months) cycling of potentially dissolved riverine nutrients tends to govern nutrient ratios and bioavailability (Isles et al., 2017).

Insights into landscape drivers of concentration-discharge patterns provided by this BLR-SOM approach can also aid water resource managers. For example, different management strategies would be warranted for each of the high-flux basin clusters for PP, based on differences in the identified export regimes. Emphasis could be placed on diverting, detaining, and attenuating storm-water flows and restoring and enhancing connections to floodplains and channel-contiguous wetlands in PP Cluster 3 (Model A2) basins, where flux is more episodic in nature, hydrologically driven and disproportionately occurring during relatively infrequent, high-magnitude runoff events. Whereas, source reduction and other best management practices to

buffer and disconnect sediment and PP source regions from the stream network would be more appropriate in PP Cluster 1 (Model D) basins characterized by greater baseline (legacy) supplies of these constituents. Similarly, DP clustering results that distinguish groups of high-flux basins by association with different land use patterns, may suggest differences in DP source types (e.g., point versus diffuse) and focus restoration or remediation efforts, accordingly. A better understanding of between-watershed differences in the functional stages of constituent export is also important in a nonstationary climate to anticipate spatially and temporally variant sensitivities to increased frequency, persistence, and intensity of storm events (Guilbert et al., 2015) and projected increases in dry summer conditions (Guilbert et al., 2014).

This data-driven, nonparametric approach to classification of export regimes can be particularly useful in an adaptive management context, as analysis is easily updated with new estimates of physical and chemical data. Computation methods (section 2.3.2) can be adapted to handle censored data (Kruschke, 2015). The Bayesian framework offers particular flexibility for study areas with sparse C-Q data. Our methods used vague priors on parameter estimates, so that the data would drive the estimates (Gelman et al., 2004). However, this technique could also be used with informative priors for watersheds with limited C-Q data. For example, analysis could apply the basin-scale posterior range for regression parameters as a prior on BLRs to estimate C-Q relationships at a subwatershed scale, provided that biogeophysical characteristics of the two scales are similar. In a temporal context, our basin-scale estimates could be used as prior information in a hierarchical model of C-Q regressions by season (subject of a pending future publication).

While application of these techniques to other hydroclimatic regions and different spatial and temporal scales would yield insights into C-Q patterns unique to those areas, the overall BLR-SOM framework and methodology should be transferable among regions. The Bayesian model is sufficiently flexible to estimate parameters for C-Q responses with multiple thresholds, and the BLR approach could be extended to model additional solutes with different C-Q patterns. With increasing availability of high-frequency concentration and discharge monitoring data from in situ sensors, automation of the BLR-SOM approach could permit near-real-time estimation of export regimes, of value to water quality management and stakeholder communities.

References

Alameddine, I., Qian, S. S., & Reckhow, K. H. (2011). A Bayesian change point-threshold model to examine the effect of TMDL implementation on the flow-nitrogen concentration relationship in the Neuse River basin. *Water Research*, *45*, 51–62. https://doi.org/10.1016/j.watres.2010.08.003

Alvarez-Guerra, M., González-Piñuela, C., Andrés, A., Galán, B., & Viguri, J. R. (2008). Assessment of Self-Organizing Map artificial neural networks for the classification of sediment quality. *Environment International*, *34*(6), 782–790. https://doi.org/10.1016/j.envint.2008.01.006

Anderson, M. J. (2001). A new method for non-parametric multivariate analysis of variance. *Austral Ecology*, *26*, 32–46. https://doi.org/10.1111/j.1442-9993.2001.01070.pp.x

Asselman, N. E. M. (2000). Fitting and interpretation of sediment rating curves. *Journal of Hydrology*, *234*, 228–248. https://doi.org/10.1016/S0022-1694(00)00253-5

Baker, V. R. (1977). Stream-channel response to floods, with examples from central Texas. *GSA Bulletin*, *88*, 1057–1071.

Basu, N. B., Destouni, G., Jawitz, J. W., Thompson, S. E., Loukinova, N. V., Darracq, A., . . . Rao, P. S. C. (2010). Nutrient loads exported from managed catchments reveal emergent biogeochemical stationarity. *Geophysical Research Letters*, *37*, L23404. https://doi.org/10.1029/2010GL045168

Basu, N. B., Thompson, S. E., & Rao, P. S. C. (2011). Hydrologic and biogeochemical functioning of intensively managed catchments: A synthesis of top-down analyses. *Water Resources Research*, *47*, W00J15. https://doi.org/10.1029/2011WR010800

Benda, L., & Dunne, T. (1997). Stochastic forcing of sediment supply to channel networks from landsliding and debris flow. *Water Resources Research*, *33*(12), 2849–2863.

Bende-Michl, U., Verburg, K., & Creswell, H. P. (2013). High-frequency nutrient monitoring to infer seasonal patterns in catchment source availability, mobilization and delivery. *Environmental Monitoring and Assessment*, *185*, 9191–9219.

Bieroza, M. Z., & Heathwaite, A. L. (2015). Seasonal variation in phosphorus concentration–discharge hysteresis inferred from high-frequency in situ monitoring. *Journal of Hydrology*, *524*, 333–347. https://doi.org/10.1016/j.jhydrol.2015.02.036

Boano, F., Harvey, J. W., Marion, A., Packman, A. I., Revelli, R., Ridolfi, L., & Wörman, A. (2014). Hyporheic flow and transport processes: Mechanisms, models, and biogeochemical implications. *Reviews of Geophysics*, *52*, 603–679. https://doi.org/10.1002/2012RG000417

Centre d'expertise hydrique Québec (2016). *Fiche signalétique de la station 030424: Centre d'expertise hydrique Québec Hydrometric Network level and flow history station database*. Retrieved from http://www.cehq.gouv.qc.ca/hydrometrie/historique_donnees/fiche_station.asp?NoStation=030424, accessed May 4, 2016

Cereghino, R., & Park, Y.-S. (2009). Review of the Self-Organizing Map (SOM) approach in water resources: Commentary. *Environmental Modelling and Software*, *24*, 945-947.

Denwood, M. J. (2016). runjags: An R package providing interface utilities, model templates, parallel computing methods and additional distributions for MCMC models in JAGS. *Journal of Statistical Software*, *71*(9), 1-25. https://doi.org/10.18637/jss.v071.i09

Doyle, M. W., Stanley, E. H., Strayer, D. L., Jacobson, R. B., & Schmidt, J. C. (2005). Effective discharge analysis of ecological processes in streams. *Water Resources Research*, *41*, W11411. https://doi.org/10.1029/2005WR004222

Dunne, T., & Black, R. D. (1970). Partial area contributions to storm runoff in a small New England watershed. *Water Resources Research*, *6*(5), 1296–1311.

Fisher, S. G., Grimm, N. B., Martı, E., Holmes, R. M., & Jones, J. B. Jr. (1998). Material spiraling in stream corridors: A telescoping ecosystem model. *Ecosystems*, *1*, 19–34. https://doi.org/10.1007/s100219900003

Franzi, D. A., Fuller, R. D., & Kramer, S. R. (2009). *A preliminary study of nonpoint source runoff in the Little Chazy River watershed, northeastern New York*. New York, NY: New York State Department of Environmental Conservation and The Nature Conservancy. Retrieved from http://www.lcbp.org/techreportPDF/chazy-npsrunoffJun09.pdf

Fytilis, N., & Rizzo, D. M. (2013). Coupling self-organizing maps with a Naıve Bayesian classifier: Stream classification studies using multiple assessment data. *Water Resources Research*, *49*, 7747–7762. https://doi.org/10.1002/2012WR013422

Gall, H. E., Park, J., Harman, C. J., Jawitz, J. W., & Rao, P. S. C. (2013). Landscape filtering of hydrologic and biogeochemical responses in managed catchments. *Landscape Ecology*, *28*, 651–664. https://doi.org/10.1007/s10980-012-9829-x

Gelman, A., Carlin, J. B., Stern, H. S., & Rubin, D. B. (2004). *Bayesian data analysis*. Boca Raton, FL: Chapman & Hall/CRC.

Gelman, A., & Rubin, D. B. (1992). Inference from iterative simulation using multiple sequences. *Statistical Science*, *7*, 457–472.

Giles, C. D., Isles, P. D. F., Manley, T., Xu, Y., Druschel, G. K., & Schroth, A. W. (2016). The mobility of phosphorus, iron, and manganese through the sediment–water continuum of a shallow eutrophic freshwater lake under stratified and mixed water-column conditions. *Biogeochemistry*, *127*, 15–34. https://doi.org/10.1007/s10533-015-0144-x

Godsey, S. E., Kirchner, J. W., & Clow, D. W. (2009). Concentration–discharge relationships reflect chemostatic characteristics of US catchments. *Hydrological Processes*, *23*, 1844–1864. https://doi.org/10.1002/hyp.7315

Guilbert, J., Beckage, B., Winter, J. M., Horton, R. M., Perkins, T., & Bomblies, A. (2014). Impacts of projected climate change over the Lake Champlain Basin in Vermont. *Journal of Applied Meteorology and Climatology*, *53*, 1861–1875. https://doi.org/10.1175/JAMC-D-13-0338.1

Guilbert, J., Betts, A. K., Rizzo, D. M., Beckage, B., & Bomblies, A. (2015). Characterization of increased persistence and intensity of precipitation in the Northeastern United States. *Geophysical Research Letters*, *42*, 1888–1893. https://doi.org/10.1002/2015GL063124

Harvey, J. W., Drummond, J. D., Martin, R. L., McPhillips, L. E., Packman, A. I., Jerolmack, D. J., . . . Tobias, C. R. (2012). Hydrogeomorphology of the hyporheic zone: Stream solute and fine particle interactions with a dynamic streambed. *Journal of Geophysical Research*, *117*, G00N11. https://doi.org/10.1029/2012JG002043

Harvey, J., & Gooseff, M. (2015). River corridor science: Hydrologic exchange and ecological consequences from bedforms to basins. *Water Resources Research*, *51*, 6893–6922. https://doi.org/10.1002/2015WR017617

Heathwaite, A. L., Sharpley, A. N., & Gburek, W. J. (2000). A conceptual approach for integrating phosphorus and nitrogen management at catchment scales. *Journal of Environmental Quality*, *29*, 158–166.

Hicks, D. M., Gomez, B., & Trustrum, N. A. (2000). Erosion thresholds and suspended sediment yields, Waipaoa River Basin, New Zealand. *Water Resources Research*, *36*(4), 1129–1142. https://doi.org/10.1029/1999WR900340

Hirsch, R. M., Moyer, D. L., & Archfield, S. A. (2010). Weighted regressions on time, discharge, and season (WRTDS), with an application to Chesapeake Bay river inputs. *Journal of American Water Resources Associations*, *46*(5), 857–880. https://doi.org/10.1111/j.1752-1688.2010.00482.x

Isles, P. D. F., Giles, C. D., Gearhart, T. A., Xu, Y., Druschel, G. K., & Schroth, A. W. (2015). Dynamic internal drivers of a historically severe cyanobacteria bloom in Lake Champlain revealed through comprehensive monitoring. *Journal of Great Lakes Research*, *41*(3), 818–829. https://doi.org/10.1016/j.jglr.2015.06.006

Isles, P. D. F., Xu, Y., Stockwell, J., & Schroth, A. W. (2017). Climate-driven changes in energy and mass inputs systematically alter nutrient concentration and stoichiometry in deep and shallow regions of Lake Champlain. *Biogeochemistry*, *133*, 201–217. https://doi.org/10.1007/s10533-017-0327-8

Jackson, W. L., & Beschta, R. L. (1982). A model of two-phase bedload transport in an Oregon Coast Range stream. *Earth Surface Processes and Landforms*, *7*, 517–527. https://doi.org/10.1002/esp.3290070602

Karwan, D. L., & Saiers, J. E. (2009). Influences of seasonal flow regime on the fate and transport of fine particles and a dissolved solute in a New England stream. *Water Resources Research*, *45*, W11423. https://doi.org/10.1029/2009WR008077

Karymbalis, E., Gaki-Papanastassiou, K., & Ferentinou, M. (2010). Fan deltas classification coupling morphometric analysis and artificial neural networks: The case of NW coast of Gulf of Corinth, Greece. *Hellenic Journal of Geosciences*, *45*, 133–146.

Kennard, M. J., Mackay, S. J., Pusey, B. J., Olden, J. D., & Marsh, N. (2010). Quantifying uncertainty in estimation of hydrologic metrics for eco-hydrological studies. *River Research and Applications*, *26*, 137–156. https://doi.org/10.1002/rra.1249

Kline, M., & Cahoon, B. (2010). Protecting river corridors in Vermont. *Journal of the American Water Resources Association*, *46*(2), 227–236. https://doi.org/10.1111/j.1752-1688.2010.00417.x

Koch, R. W., & Smillie, G. M. (1986). Bias in hydrologic prediction using log-transformed regression models. *Water Resources Bulletin*, *22*(5), 717–723. https://doi.org/10.1111/j.1752-1688.1986.tb00744.x

Kohonen, T. (1990). The Self-Organizing Map. *Proceedings of the IEEE*, *78*(9), 1464–1480.

Kohonen, T. (2001). *Self-organizing maps* (3rd ed.). Berlin, Germany: Springer.

Kohonen, T. (2013). Essentials of the Self-Organizing Map. *Neural Networks*, *37*, 52–65. https://doi.org/10.1016/j.neunet.2012.09.018

Kondolf, G. M. (1997). PROFILE: Hungry water: Effects of dams and gravel mining on river channels. *Environmental Management*, *21*(4), 533–551. https://doi.org/10.1007/s002679900048

Krishnaswamy, J., Lavine, M., Richter, D. D., & Korfmacher, K. (2000). Dynamic modeling of long term sedimentation in the Yadkin River Basin. *Advances in Water Resources*, *23*(8), 881–892. https://doi.org/10.1016/S0309-1708(00)00013-0

Kruschke, J. K. (2015). *Doing Bayesian data analysis: A tutorial with R, JAGS, and Stan* (2nd ed.). Boston, MA: Academic Press.

Lawler, D. M., Petts, G. E., Foster, I. D. L., & Harper, S. (2006). Turbidity dynamics during spring storm events in an urban headwater river system: The Upper Tame, West Midlands, UK. *Science of the Total Environment*, *360*, 109–126. https://doi.org/10.1016/j.scitotenv.2005.08.032

Ley, R., Casper, M. C., Hellebrand, H., & Merz, R. (2011). Catchment classification by runoff behaviour with self-organizing maps (SOMs). *Hydrology and Earth Systems Science*, *15*, 2947–2962. https://doi.org/10.5194/hess-15-2947-2011

Lloyd, C. E., Freer, J. E., Johnes, P. J., & Collins, A. L. (2016). Using hysteresis analysis of high-resolution water quality monitoring data, including uncertainty, to infer controls on nutrient and sediment transfer in catchments. *Science of the Total Environmental*, *543*(Part A), 388–404. https://doi.org/10.1016/j.scitotenv.2015.11.028

Lumia, R., Freehafer, D. A., & Smith, M. J. (2006). *Magnitude and frequency of floods in New York* (U.S. Geol. Surv. Sci. Invest. Rep. 2006–5112, 152 p.). Washington, DC: U.S. Geological Survey.

Mangiameli, P., Chen, S. K., & West, D. (1996). A comparison of SOM neural network and hierarchical clustering methods. *European Journal of Operational Research*, *93*(2), 402–417. https://doi.org/10.1016/0377-2217(96)00038-0

McClain, M. E., Boyer, E. W., Dent, C. L., Gergel, S. E., Grimm, N. B., Groffman, P. M., . . . Pinay, G. (2003). Biogeochemical hot spots and hot moments at the interface of terrestrial and aquatic ecosystems. *Ecosystems*, *6*, 301–312. https://doi.org/10.1007/s10021-003-0161-9

McDonnell, J. J., Sivapalan, M., Vache, K., Dunn, S., Grant, G., Haggerty, R., . . . Weiler, M. (2007). Moving beyond heterogeneity and process complexity: A new vision for watershed hydrology. *Water Resources Research*, *43*, W07301. https://doi.org/10.1029/2006WR005467

Meade, R. H. (1982). Sources, sinks and storage of river sediment in the Atlantic drainage of the United States. *Journal of Geology*, *90*, 235–252.

Medalie, L. (2013). *Concentration, flux, and the analysis of trends of total and dissolved phosphorus, total nitrogen, and chloride in 18 tributaries to Lake Champlain, Vermont and New York, 1990–2011* (U.S. Geol. Surv. Sci. Invest. Rep. 2013–5021, 31 p.). Washington, DC: U.S. Geological Survey. Retrieved from http://pubs.usgs.gov/sir/2013/5021/

Medalie, L. (2014). *Concentration and flux of total and dissolved phosphorus, total nitrogen, chloride, and total suspended solids for monitored tributaries of Lake Champlain, 1990–2012* (U.S. Geol. Surv. Open File Rep. 2014–1209, 21 p.). Washington, DC: U.S. Geological Survey. Retrieved from https://doi.org/10.3133/ofr20141209

Medalie, L., Hirsch, R. M., & Archfield, S. A. (2012). Use of flow-normalization to evaluate nutrient concentration and flux changes in Lake Champlain tributaries, 1990–2009. *Journal of Great Lakes Research*, *38*, 58–67. https://doi.org/10.1016/j.jglr.2011.10.002

Meybeck, M., & Moatar, F. (2012). Daily variability of river concentrations and fluxes: Indicators based on the segmentation of the rating curve. *Hydrological Processes*, *26*, 1188–1207. https://doi.org/10.1002/hyp.8211

Moatar, F., Abbott, B. W., Minaudo, C., Curie, F., & Pinay, G. (2017). Elemental properties, hydrology, and biology interact to shape concentration-discharge curves for carbon, nutrients, sediment, and major ions. *Water Resources Research*, *53*, 1270–1287. https://doi.org/10.1002/2016WR019635

Moyeed, R. A., & Clark, R. T. (2005). The use of Bayesian methods for fitting rating curves, with case studies. *Advances in Water Resources*, *28*, 807–818. https://doi.org/10.1016/j.advwatres.2005.02.005

Mulholland, P. J., Marzolf, E. R., Webster, J. R., Hart, D. R., & Hendricks, S. P. (1997). Evidence that hyporheic zones increase heterotrophic metabolism and phosphorus uptake in forest streams. *Limnology and Oceanography*, *42*(3), 443–451.

Musolff, A., Schmidt, C., Selle, B., & Fleckenstein, J. H. (2015). Catchment controls on solute export. *Advances in Water Resources*, *86*, 133–146. https://doi.org/10.1016/j.advwatres.2015.09.026

Nanson, G. C. (1986). Episodes of vertical accretion and catastrophic stripping: A model of disequilibrium floodplain development. *Geological Society of American Bulletin*, *97*, 1467–1475. https://doi.org/10.1130/0016-7606(1986)97<1467:EOVAAC>2.0.CO;2

Nash, D. B. (1994). Effective sediment-transporting discharge from magnitude-frequency analysis. *Journal of Geology*, *102*(1), 79–95. https://doi.org/10.1086/629649

Oksanen, J., Blanchet, F. G., Friendly, M., Kindt, R., Legendre, P., McGlinn, D., . . . Wagner, H. (2017). *vegan: Community ecology package. R package version 2.4-3*. Retrieved from https://CRAN.R-project.org/package=vegan

Olson, S. A. (2014). *Estimation of flood discharges at selected annual exceedance probabilities for unregulated, rural streams in Vermont, with a section on Vermont regional skew regression, by A. G. Veilleux* (U.S. Geol. Surv. Sci. Invest. Rep. 2014–5078, 27 p.). Washington, DC: U.S. Geological Survey. Retrieved from https://doi.org/10.3133/sir20145078

Park, Y.-S., Cereghino, R., Compin, A., & Lek, S. (2003). Applications of artificial neural networks for patterning and predicting aquatic insect species richness in running waters. *Ecological Modelling*, *160*, 265–280. https://doi.org/10.1016/j.ecoinf.2015.08.011

Pearce, A. R., Rizzo, D. M., & Mouser, P. J. (2011). Subsurface characterization of groundwater contaminated by landfill leachate using microbial community profile data and a non-parametric decision making process. *Water Resources Research*, *47*, W06511. https://doi.org/10.1029/2010WR009992

Pearce, A. R., Rizzo, D. M., Watzin, M. C., & Druschel, G. K. (2013). Unraveling associations between Cyanobacteria blooms and in-lake environmental conditions in Missisquoi Bay, Lake Champlain, USA, using a modified Self-Organizing Map. *Environmental Science and Technology*, *47*, 14267–14274. https://doi.org/10.1021/es403490g

Pizzuto, J. E. (2014). Long-term storage and transport length scale of fine sediment: Analysis of a mercury release into a river. *Geophysical Research Letters*, *41*, 5875–5882. https://doi.org/10.1002/2014GL060722

Plummer, M. (2003). *JAGS: A program for analysis of Bayesian graphical models using Gibbs sampling*. Paper presented at Proceedings of the 3rd international workshop on distributed statistical computing (dsc 2003), Vienna, Austria.

Plummer, M. (2016). *Rjags: Bayesian graphical models using MCMC. R package version 4–6*. Retrieved from https://CRAN.R-project.org/package=rjags

Plummer, M., Best, N., Cowles, K., & Vines, K. (2006). CODA: Convergence diagnosis and output analysis for MCMC, *R News*, 6, 7–11. Retrieved from https://www.r-project.org/doc/Rnews/Rnews_2006-1.pdf

Qian, S. S., & Cuffney, T. F. (2012). To threshold or not to threshold? That's the question. *Ecological Indicators*, *15*, 1–9. https://doi.org/10.1016/j.ecolind.2011.08.019

Qian, S. S., Reckhow, K. H., Zhai, J., & McMahon, G. (2005). Nonlinear regression modeling of nutrient loads in streams: A Bayesian approach. *Water Resources Research*, *41*, W07012. https://doi.org/10.1029/2005WR003986

Qian, S. S., & Richardson, C. J. (1997). Estimating the long-term phosphorus accretion rate in the Everglades: A Bayesian approach with risk assessment. *Water Resources Research*, *33*(7), 1681–1688. https://doi.org/10.1029/97WR00997

R Core Team (2016). *R: A language and environment for statistical computing*. Vienna, Austria: R Foundation for Statistical Computing. Retrieved from http://www.R-project.org/

Randall, A. D. (1996). *Mean annual runoff, precipitation, and evapotranspiration in the glaciated northeastern United States, 1951–1980* (U.S. Geol. Surv. Open File Rep. 96–395). Washington, DC: U.S. Geological Survey.

Reid, I., Bathurst, J. C., Carling, P. A., Walling, D. E., & Webb, B. W. (1997). Sediment erosion, transport and deposition. In C. R. Thorne, R. D. Hey, & G. P. Williams (Eds.), *Applied fluvial geomorphology for river engineering and management* (pp. 95–135). New York, NY: John Wiley.

Roy, N. G., & Sinha, R. (2014). Effective discharge for suspended sediment transport of the Ganga River and its geomorphic implication. *Geomorphology*, *227*, 18–30. https://doi.org/10.1016/j.geomorph.2014.04.029

Ryan, S. E., Porth, L. S., & Troendle, C. A. (2002). Defining phases of bedload transport using piecewise regression. *Earth Surface Processes and Landforms*, *27*, 971–990. https://doi.org/10.1002/esp.387

Schmelter, M. L., Erwin, S. O., & Wilcock, P. R. (2012). Accounting for uncertainty in cumulative sediment transport using Bayesian statistics. *Geomorphology*, *175–176*(15), 1–13. https://doi.org/10.1016/j.geomorph.2012.06.012

Shanley, J. B., & Denner, J. C. (1999). The hydrology of the Lake Champlain Basin. In T. O. Manley and P. L. Manley (Eds.), *Lake Champlain in transition: From research toward restoration* (pp. 41–66). Washington, DC: American Geophysical Union. Retrieved from https://doi.org/10.1029/WS001p0041

Shanley, J. B., McDowell, W. H., & Stallard, R. F. (2011). Long-term patterns and short-term dynamics of stream solutes and suspended sediment in a rapidly weathering tropical watershed. *Water Resources Research*, *47*, W07515. https://doi.org/10.1029/2010WR009788

Skalak, K., & Pizzuto, J. (2010). The distribution and residence time of suspended sediment stored within the channel margins of a gravel-bed bedrock river. *Earth Surface Processes and Landforms*, *35*, 435–446. https://doi.org/10.1002/esp.1926

Smeltzer, E., Shambaugh, A. D., & Stangel, P. (2012). Environmental change in Lake Champlain revealed by long-term monitoring. *Journal of Great Lakes Research*, *38*, 6–18. https://doi.org/10.1016/j.jglr.2012.01.002

Spiegelhalter, D. J., Best, N. G., Carlin, B. P., & van der Linde, A. (2002). Bayesian measures of model complexity and fit (with discussion). *Journal of the Royal Statistical Society*, *64*, 583–639. https://doi.org/10.1111/1467-9868.00353

Stewart, D. P., & MacClintock, P. (1969). *The surficial geology and pleistocene history of Vermont* (Bulletin No. 31). Montpelier, VT: Vermont Geological Survey.

Stojkovica, M., Simic, V., Milosevic, D., Mancev, D., & Penczak, T. (2013). Visualization of fish community distribution patterns using the self-organizing map: A case study of the Great Morava River system (Serbia). *Ecological Modelling*, *248*, 20–29. https://doi.org/10.1016/j.ecol-model.2012.09.014

Stow, C. A., Reckhow, K. H., & Qian, S. S. (2006). A Bayesian approach to retransformation bias in transformed regression. *Ecology*, *87*(6), 1472–1477. https://doi.org/10.1890/0012-9658(2006)87[1472:ABATRB]2.0.CO;2

Syvitski, J. P., Morehead, M. D., Bahr, D. B., & Mulder, T. (2000). Estimating fluvial sediment transport: The rating parameters. *Water Resources Research*, *36*(9), 2747–2760. 10.1029/2000WR900133.

Thompson, S. E., Basu, N. B., Lascurain, J. Jr., Aubeneau, A., & Rao, P. S. C. (2011). Relative dominance of hydrologic versus biogeochemical factors on solute export across impact gradients. *Water Resources Research*, *47*, W00J05. https://doi.org/10.1029/2010WR009605

Todini, E. (2007). Hydrological catchment modelling: Past, present, and future. *Hydrology and Earth Systems Science*, *11*(1), 468–482. https://doi.org/10.5194/hess-11-468-2007

Toone, J., Rice, S., & Piégay, H. (2014). Spatial discontinuity and temporal evolution of channel morphology along a mixed bedrock-alluvial river, upper Drôme River, southeast France: Contingent responses to external and internal controls. *Geomorphology*, *205*, 5–16. https://doi.org/10.1016/j.geomorph.2012.05.033

Tran, L. T., Knight, C. G., O'neill, R. V., Smith, E. R., & O'connell, M. (2003). Self-Organizing Maps for integrated environmental assessment of the Mid-Atlantic region. *Environmental Management*, *31*(6), 822–835.

Trimble, S. W. (1997). Contribution of stream channel erosion to sediment yield from an urbanizing watershed. *Science*, *278*, 1442–1444. https://doi.org/10.1126/science.278.5342.1442

Troy, A., Wang, D., Capen, D., O'neil-Dunne, J., & MacFaden, S. (2007). *Updating the Lake Champlain basin land use data to improve prediction of phosphorus loading* (Tech. Rep. 54). Grand Isle, VT: Lake Champlain Basin Program. Retrieved from http://www.lcbp.org/techreportPDF/54_LULC-Phosphorus_2007.pdf

USGS (2016). *National water information system*. Retrieved from http://waterdata.usgs.gov/vt/nwis/rt

Vesanto, J., & Alhoniemi, E. (2000). Clustering of the Self-Organizing Map. *IEEE Transactions on Neural Networks*, *11*(3), 586–600.

Vesanto, J., Himberg, J., Alhoniemi, E., & Parhankangas, J. (2000). *SOM toolbox for Matlab 5* (Tech. Rep. A57). Helsinki, Finland: Neural Networks Research Centre, Helsinki University of Technology.

Vigiak, O., & Bende-Michl, U. (2013). Estimating bootstrap and Bayesian prediction intervals for constituent load rating curves. *Water Resources Research*, *49*, 8565–8578. https://doi.org/10.1002/2013WR013559

Vogel, R. M., Rudolph, B. E., & Hooper, R. P. (2005). Probabilistic behavior of water-quality loads. *Journal of Environmental Engineering*, *131*(7), 1081–1089. https://doi.org/10.1061/(ASCE)0733-9372(2005)131:7(1081)

VTDEC (2015). *Lake Champlain long-term water quality and biological monitoring program: Program description*. Retrieved from https://anr-web.vermont.gov/dec/_dec/LongTermMonitoringTributary.aspx

Walling, D. E. (1977). Assessing the accuracy of suspended sediment rating curves for a small basin. *Water Resources Research, 13(3)*, 531–538.

Walling, D. E., & He, Q. (1999). Using fallout lead-210 measurements to estimate soil erosion on cultivated land. *Soil Science Society of American Journal*, *63*, 1404–1412. https://doi.org/10.2136/sssaj1999.6351404x

Walling, D. E., Owens, P. N., & Leeks, G. J. L. (1999). Fingerprinting suspended sediment sources in the catchment of the River Ouse, Yorkshire, UK. *Hydrological Processes*, *13*, 955–975.

Wang, H., Yang, Z., Wang, Y., Saito, Y., & Liu, J. P. (2008). Reconstruction of sediment flux from the Changjiang (Yangtze River) to the sea since the 1860s. *Journal of Hydrology*, *349*, 318–332. https://doi.org/10.1016/j.jhydrol.2007.11.005

Ward, J. V. (1989). The four-dimensional nature of lotic ecosystems. *Journal North American Benthological Society*, *8*, 2–8. https://doi.org/10.2307/1467397

Warrick, J. A. (2014). Trend analyses with river sediment rating curves. *Hydrological Processes*, *29*(6), 936–949. https://doi.org/10.1002/hyp.10198

Watson, K., Ricketts, T., Galford, G., Polasky, S., & O'niel-Dunne, J. (2016). Quantifying flood mitigation services: The economic value of Otter Creek wetlands and floodplains to Middlebury, VT. *Ecological Economics*, *130*, 16–24. https://doi.org/10.1016/j.ecolecon.2016.05.015

Wehrens, R., & Buydens, L. M. C. (2007). Self- and super-organising Maps in R: The kohonen package. *Journal of Statistical Software*, *21*(5), 1–19. Retrieved from https://www.jstatsoft.org/index

Williams, G. P., & Wolman, M. G. (1984). *Downstream effects of dams on alluvial rivers* (U.S. Geol. Surv. Prof. Pap. 1286, 83 p.). Washington, DC: U.S. Geological Survey.

Withers, P. J. A., & Jarvie, H. P. (2008). Delivery and cycling of phosphorus in rivers: A review. *Science of the Total Environment*, *400*, 379–395. https://doi.org/10.1016/j.scitotenv.2008.08.002

Wohl, E., & Beckman, N. D. (2014). Leaky rivers: Implications of the loss of longitudinal fluvial disconnectivity in headwater streams. *Geomorphology*, *205*, 27–35. https://doi.org/10.1016/j.geomorph.2011.10.022

Wolman, M. G., & Gerson, R. (1978). Relative scales of time and effectiveness of climate in watershed geomorphology. *Earth Surface Processes and Landforms*, *3*, 189–208. https://doi.org/10.1002/esp.3290030207

Xu, Y., Schroth, A. W., Isles, P. D. F., & Rizzo, D. M. (2015a). Quantile regression improves models of lake eutrophication with implications for ecosystem-specific management. *Freshwater Biology*, *60*, 1841–1853. https://doi.org/10.1111/fwb.12615

Xu, Y., Schroth, A. W., & Rizzo, D. M. (2015b). Developing a 21st century framework for lake-specific eutrophication assessment using quantile regression. *Limnology and Oceanography*, *13*, 237–249. https://doi.org/10.1002/lom3.10021

Yellen, B., Woodruff, J. D., Kratz, L. N., Mabee, S. B., Morrison, J., & Martini, A. M. (2014). Source, conveyance and fate of suspended sediments following Hurricane Irene. New England, USA. *Geomorphology*, *226*, 124–134. https://doi.org/10.1016/j.geomorph.2014.07.028

Zhang, Q., Harman, C. J., & Ball, W. P. (2016). An improved method for interpretation of riverine concentration-discharge relationships indicates long-term shifts in reservoir sediment trapping. *Geophysical Research Letters*, *43*, 10215–10,224. https://doi.org/10.1002/2016GL069945

Zia, A., Bomblies, A., Schroth, A. W., Koliba, C., Isles, P. D. F., Tsai, Y., . . . Van Houten, J. (2016). Coupled impacts of climate and land use change across a river–lake continuum: Insights from an integrated assessment model of Lake Champlain's Missisquoi Basin, 2000–2040. *Environmental Research Letters*, *11*, 114026. https://doi.org/10.1088/1748-9326/11/11/114026